January 2012

Development Of Ionic Liquid Swelled Poly-Electrolyte Membranes For Use In Dye-Sensitized Solar Cells

Eric D. Schmid

DEVELOPMENT OF
IONIC LIQUID SWELLED POLY-ELECTROLYTE MEMBRANES
FOR USE IN DYE-SENSITIZED SOLAR CELLS

by

Eric D. Schmid
Bachelor of Science, Jamestown College, 2009

A Thesis

Submitted to the Graduate Faculty

of the

University of North Dakota

in partial fulfillment of the requirements

for the degree of

Master of Science

Grand Forks, North Dakota
May
2012

This thesis, submitted by Eric D. Schmid in partial fulfillment of the requirements for the Degree of Master of Science from the University of North Dakota, has been read by the Faculty Advisory Committee under whom the work has been done and is hereby approved.

Dr. Edward Koloda -- Chairperson

Dr. Brian Tande

Dr. Frank Bowman

This thesis meets the standards for appearance, conforms to the style and format requirements of the Graduate School of the University of North Dakota, and is hereby approved.

Wayne Swisher, PhD
Dean of the Graduate School

Date

PERMISSION

Title Development of Ionic Liquid Swelled Poly-Electrolyte Membranes for use in Dye-Sensitized Solar Cells

Department Chemical Engineering

Degree Master of Science

In presenting this thesis in partial fulfillment of the requirements for a graduate degree from the University of North Dakota, I agree that the library of this University shall make it freely available for inspection. I further agree that permission for extensive copying for scholarly purposes may be granted by the professor who supervised my thesis work or, in his absence, by the chairperson of the department or the dean of the Graduate School. It is understood that any copying or publication or other use of this thesis or part thereof for financial gain shall not be allowed without my written permission. It is also understood that due recognition shall be given to me and to the University of North Dakota in any scholarly use which may be made of any material in my thesis.

Signature 

Date April 24, 2012

TABLE OF CONTENTS

LIST OF FIGURES

LIST OF TABLES

ACKNOWLEDGEMENTS

The author of this paper wishes to acknowledge North Dakota Experimental Program to Stimulate Competitive Research (EPSCoR) for funding the beginning stages of this project. He also wishes to thank the research team at South Dakota State University (Curtiss Kovash, Jr., Josh Kofford, and Dr. Brian Logue) for their assistance in the initial stages of cell fabrication, and for their kind donation of important materials and supplies.

Additionally, thanks are bestowed upon my family for their full support and my friends for their encouragement throughout my ceaseless academic career. Nothing could have been accomplished without them! He also wishes to acknowledge his professors, teachers, and mentors for their dedication to teaching and for the advice they have always been ready to share with him.

Finally, someone once said that as “smart people, we should be able to figure this out!” Notice the emphasis on “we” – it is plural! That being said, there is always help if you simply are willing to ask for it.

Now off to work you go, and good luck with your research!

This thesis is dedicated to

Parents, Teachers, and Friends

that still ask

“Are you still in school? When are you going to get a job?”

Thanks for the support!

ABSTRACT

The flexible design, inexpensive nature, and relatively high cell performance of dye sensitized solar cells make these devices very appealing as the next generation of photovoltaic modules. However, a trade-off exists between cell performance and cell lifetime due to limitations in material structure and device construction. The organic solvents used in cell electrolytes are volatile, making device sealing difficult and cell performance short lived. Solid polymer electrolytes are much more stable and easier to process, but ionic diffusion is greatly hindered, leading to substantially lower cell performance. It is hypothesized that a swelled polymer electrolyte, composed of an ionic liquid and a polyelectrolyte membrane, can approach the performance of a liquid electrolyte while achieving the stability of a solid state electrolyte.

Poly(diallyldimethylammonium iodide), poly(DADMAI), was obtained from poly(diallyldimethylammonium chloride), poly(DADMAC), via a simple ion exchange of chloride for iodide. The working hypothesis is that since polyelectrolyte materials are able to facilitate charge transfer quite well, incorporating iodide into the stable polyelectrolyte structure will result in a high number of iodide ions available for reaction and ionic conductivity. Additionally, the stability and performance of the electrolyte will be further enhanced due to the combination of ionic liquid and solid polyelectrolyte membrane. It is also expected that the ionic liquid will maintain higher conductivity through the polymer membrane without increasing the volatility of the electrolyte (because ionic liquids have low vapor pressures), thus maintaining the sought after cell stability without hindering cell performance. This combination may provide

a novel method of achieving both high performance and high stability compared to similar polymer gel electrolytes.

The preliminary experimental design investigated the significance of the polyelectrolyte molecular weight, ionic liquid alkyl chain length, and the loading ratio of ionic liquid to polyelectrolyte for poly(DADMAC) alone. Insignificant factors were trimmed from the design and the study resumed using poly(DADMAI). The results were then combined and highest performing dye-sensitized solar cell were determined and verified.

The loading ratio was determined to be insignificant and was removed from the secondary experimental design. It was determined that <100,000 g/mol poly(DADMAI) combined with 1-hexyl-3-imidazolium iodide ionic liquid achieved the highest power conversion efficiency (1.60%). These cells were replicated and the optimized conditions confirmed.

It was shown that the poly(DADMAI) polymer membranes can be combined with an ionic liquid electrolyte and achieve notable, although lower, power conversion efficiencies relative to acetonitrile electrolyte dye-sensitized solar cells. Preliminary indications show these polymer membrane electrolytes maintain greater than 40% of their initial power output over a 45 day span, indicating a much more stable solar cell design relative to acetonitrile electrolyte solar cells. Now that these relatively inexpensive cells have demonstrated the ability to maintain a sustained electric current, future work can be continued to examine the use of these membranes in future solar cell optimization.

CHAPTER I

AN INTRODUCTION TO SOLAR CONCEPTS

Due to the combined effect of an exponentially increasing global population and continuing growth of industry by countries around the world, the annual energy demand of human society is expected to double by the year 2050, and triple by the end of this century [1]. Speculations regarding the lack of future fossil fuels and their corresponding high price have led to an increased interest in renewable energy markets and the advent of the "Sustainable Revolution." A variety of natural energy sources have been evaluated for quenching human energy thirst, including hydropower, geothermal, wind, solar, and bio-fuel sources. Solar energy may be the most obvious solution to decreasing humanity's dependence upon fossil fuels simply because it is the most readily available natural energy source to the majority of the global population. However, harnessing the energy of the sun has proven to be more expensive than the average consumer is willing to pay for, due primarily to the high cost of achieving the ultra-pure silicon (99.9999%) needed to make conventional silicon solar panels. Therefore, the solution to the energy crisis involves solar technology that not only demonstrates high energy conversion efficiency and reliability, but also is relatively inexpensive compared to current photovoltaic module technology.

The current market trend in photovoltaic modules relies heavily upon the sale of high purity silicon glass sheets doped with boron and phosphorus. These modules are the most common form of solar technology, and are used in solar home systems for generating electricity

and as external power supplies in niche applications. While these doped silicon solar cells are reliable and are the most efficient photovoltaic technology available, the final average cost can reach thousands of dollars (USD) per kilowatt rating of the system [2]. Even though this price per power has been reduced substantially in recent years, it is still much higher than that of current coal fired electrical power plant energy costs. The price of residential electricity was reported at $0.116 per kilowatt hour in 2010, resulting in an average monthly bill of $110.55 across the United States [3]. A home solar power system, well designed to meet the 2010 average electricity consumption, would cost approximately $20,000, making the investment payback time almost 20 years. Solar devices like these will not be sought after by the majority of consumers until their cost is competitive with fossil fuel driven electricity.

However, there is significant research being conducted around the world in the field of thin film solar devices. Although there are many variations, the concept is to produce micro-thin solar films of cheap, readily available materials at minimal cost. Research has progressed in several directions, including micro-thin amorphous silicon ribbons, nano-thin conducting polymers, micro-thin metallic semiconductor films, concentrator solar devices, tandem solar cells utilizing an expanded working range of solar radiation, and micro-thin dye-sensitized oxides [4, 5]. Although the prominence of each cell type can be debated, it is feasible that the future of solar technology lies in the realm of the dye-sensitized solar cell.

Dye-sensitized solar cells were inspired and designed according to the most effective, if not the most efficient, energy system in nature – plant photosynthesis. Developed in 1991 by Michael Gratzel, et. al., several material components are arranged to create an energetically favorable electron transfer process which regenerates itself at the completion of the electronic circuit [6]. The basic design concept utilizes a solar absorbing dye which is soaked onto a thin conducting oxide film, a regenerative reduction-oxidation electrolyte, and a catalytic counter

electrode surface, all of which is sandwiched between two conductive substrates. Since its origin, many research groups have attempted to optimize specific sets of variables in almost every conceivable format while maintaining this general design schematic. Investigations have resulted in several revolutionary concepts in the field, including the development of inexpensive flexible polymer substrates, highly conductive polymeric materials, ionic liquid based electrolytes, functionalized catalytic carbon nanotubes, and many of the deposition and fabrication techniques used to manufacture the functioning device on a semi-large scale [7, 8].

The flexible design, inexpensive nature, and relatively high cell performance of dye sensitized solar cells make these devices very appealing as the next generation of photovoltaic modules. However, a trade-off exists between cell performance and cell lifetime due to limitations in material structure and device construction. Although ionic conductivity is readily achieved, electrolytes using organic solvents are highly volatile, making device sealing difficult and cell performance short lived. The depletion of iodide in recombinant side reactions has also resulted in cell degradation. Solid polymer electrolytes are much more stable and easier to process, but ionic diffusion is greatly hindered, leading to substantially lower cell performance parameters. It is hypothesized that an optimized polymer electrolyte, composed of a polyelectrolyte swelled with ionic liquid, can approach the performance of a liquid electrolyte while maintaining the stability of a solid-state electrolyte.

The polymer poly(DADMAC) was chosen due to its availability, high solubility in water, and inexpensive nature. An ion exchange was devised using a commonly available iodide salt to increase iodide content in the swelled polyelectrolyte. Hypothetical manufacturing concepts include a spray-on polymer solution (in water), dehydration, and a spray-on ionic liquid electrolyte, making fabrication cheap and fitting to roll-to-roll processing concepts. Roll-to-roll design strategies make use of current manufacturing principles that are easily manipulated in

new thin film polymer projects, and can achieve high volumetric output per cost compared to other production technologies. The inexpensive nature, ease of fabrication principles, and use of an environmentally friendly polymer deposition solvent make the conceptual design of this scale-up facility very appealing. First, a proof-of-concept study must be performed to determine the ability of this polyelectrolyte to achieve high performance and improved stability as a dye-sensitized solar cell electrolyte.

CHAPTER II

BACKGROUND TO DYE-SENSITIZED SOLAR CELL RESEARCH

Dye-sensitized Solar Cell Design and Functioning

Solar technology has developed in several different directions over the last few decades and it is hoped traditional doped-silicon panels can soon be replaced with any of the cheaper thin-film solar devices being developed in laboratories around the world. These new solar materials include all-organic and polymeric thin films, micro-thin silicon layers, inorganic semiconductor photovoltaics (including, but not limited to, cadmium, telluride, copper, indium, gallium, selenide, and sulfur), quantum dot devices, and dye-sensitized solar cells [4]. Of these, dye-sensitized solar cells (DSSC) are thought to have the most potential in becoming mainstream photovoltaic devices due to their relative simplicity and ease of material procurement (which lead to lower overall cost), and their ability to integrate with energy conversion and storage devices [1, 4, 6].

Photoconductivity was first observed on high purity crystalline anthracene in the early 1900's [9]. As the search for photovoltaic materials evolved in the 1950's, porphyrins and phtalocyanines were quickly identified as good photoconductive materials and have been investigated for solar applications ever since [9]. These compounds are easy to prepare and highly colored in a variety of shades depending on the metal ions with which the structures may be complexed. Cyanine dyes are still widely used in dye-sensitized solar cells, especially when exploring all-natural dye photochemical properties. In fact, the all-natural process of

photosynthesis is what led to the conceptual design and eventual production of the first dye-sensitized solar cell in 1991. Dye-sensitized solar cells are comprised of several components arranged in a manner to mimic the natural energy transfer process found in photosynthesis. While the general cell design has not changed since the initial development in 1991, the development and optimization of each internal component has led to advancements in cell materials, fabrication techniques, longevity, and overall performance [6]. When tested under global air mass 1.5 specifications (AM1.5, 1000 W/m^2, 25° C) and compared to traditional silicon solar cells (which can achieve about twenty percent efficiency at converting solar energy into electrical energy), third generation dye-sensitized solar cells are achieving approximately ten percent power conversion efficiency, but with limited cell stability and short cell lifetimes [6]. Until December of 2011, the dye-sensitized power conversion efficiency record, verified by NREL under global AM 1.5 spectral conditions at 25 °C, was 10.4% and was held by Sharp Corporation. The cell had an area of 1.004 cm^2, open circuit voltage of 0.729 V, current density of 22 mA/cm^2, and a 65.2% fill factor [7]. The new record, produced in 2011 by original cell designer Michael Gratzel, had an open circuit voltage of 0.935 V, short circuit current density of 17.66 mA/cm^2, and a 74% fill factor, which resulted in a 12.3% power conversion efficiency [10].

The general cell design (depicted in Figure 1, following page) consists of a thin transparent conducting oxide layer (most commonly anatase titanium dioxide, TiO_2) deposited on a conductive doped-tin oxide glass slide substrate. After deposition and thermal drying of the oxide, a dye is adsorbed onto the surface of the thin conducting oxide particles. This dye may be organic, such as blueberry or raspberry dye, but it is most commonly an inorganic ruthenium complex. The backside glass slide is coated with a catalytic electron transport material, usually platinum or carbon nanotubes, to produce a counter electrode which facilitates electron transport between returning current and internal electrolytic material. In between these two

slides, a reduction-oxidation electrolyte in organic solvent is “sandwiched” or injected. The most common reduction-oxidation electrolyte consists of iodide (I^-) and tri-iodide (I_3^-) ions in acetonitrile.

Each component plays a specific role in the electron transfer process. When an incident photon passes through the thin conducting oxide layer and is absorbed by the dye complex, the photonic energy is transferred to the outermost dye electrons. This energized electron, or exciton, is relayed to the highest occupied molecular orbital (HOMO) level of the dye, where it dissociates into an electron-hole pair. This electron is then injected into the conduction band of the thin conducting oxide to be drawn off as external current. Immediately after exciton

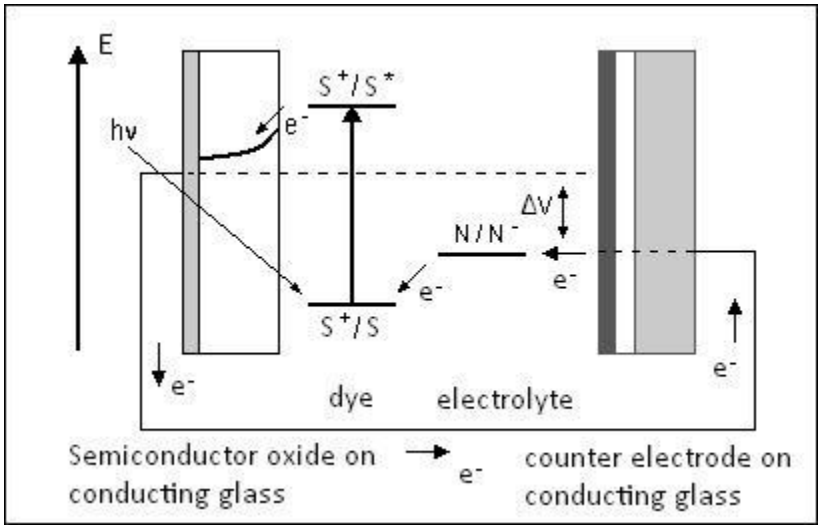

Figure 1. Dye-Sensitized Solar Cell Materials, Construction, and Electron Transfer [6]

dissociation, the reduction-oxidation (redox) iodide reactant (I^-) donates an electron to fill the vacancy in the oxidized dye, reducing the dye to its original state. The product of the redox reaction, tri-iodide (I_3^-), diffuses through the organic solvent to the counter electrode surface. There it reacts with a re-entering external current electron to regenerate the redox reactant. In theory, all materials have been restored to their original state, the circuit is complete, and external current has been drawn to power a device. In reality, there are many inhibitors,

resistances, and possible routes of electron-hole recombination that prevent this cycle from performing perfectly. This process and the materials used in a standard dye-sensitized solar cell are modeled in Figure 1. Arrows depict the desired route of energy movement throughout the cell.

Generated current is dependent upon the ability of electrons to effectively transfer throughout each stage of the device, while voltage is dependent upon the difference between the Fermi energy levels of the electron in the semiconductor electrode and the redox potential of the electrolyte [11]. There are two requirements of solar devices: charge generation and charge transport. These are met in two different stages. The exciton charge generation and separation both occur in the thin oxide semiconductor-dye interface, while the ionic charge transport is accomplished by the semiconductor and electrolytic solution [12, 13]. This has also been modeled in simple electrical simulations, which were then used to calculate the expected current density, optical properties, and integrated power loss [14, 15]. An important distinction between silicon solar devices and organic thin film solar cells occurs in the mechanism of electron transport. Silicon solar cell electron transport is chiefly driven by an electrical gradient at the electron-doped – electron-deficient heterojunction (also called a p-n junction) which results from an immediate electron-hole pair formation upon light absorption [16, 17]. Thin film solar cell electron transport is the result of exciton generation and diffusion, where both generation and diffusion must occur before the electron-hole pair can separate [17]. The implication of this difference is that thin film cells are hindered by the diffusion of an exciton through materials in the cell, while silicon cells offer essentially no resistance. This results in drastic differences in power capabilities. Illumination of a thin solar film results in the absorption of photons, whose greater-than-bandgap energy is then used to generate excited electrons. The energy of the exciton brings the electron into the conduction band of the semiconductor oxide and leaves a positively

charged vacant hole behind. This excitonic pair can be thought of as diffusing in opposite directions; the electron through the semiconductor and out of the cell as external current and the positive vacancy to the electrolyte, where it is available to oxidize a reduced state ion in the electrolytic solution [16]. The positively charged hole only "moves" because it continues to be filled with flowing electrons from different cell components. As a result of electron and hole flow, internal cell reactions occur. Of primary importance is the iodide and tri-iodide redox electrolyte, which achieves ionic transport by the concentration gradient of respective ions at the dye-electrolyte interface and the counter electrode. This gradient results from the complementary flow of electrons in one direction and holes in the other. The dye-sensitized solar cell is a complex combination of mechanisms working together, rather than a solar induced electrical gradient pushing electrons as current.

These cells are the result of several components which work together by each performing a specific mechanistic task. Each component mechanism may contribute to or hinder a high power conversion efficiency based on the fabrication technique and material properties. If just one mechanism functions poorly, the overall cell operation suffers from this limitation. Of particular importance is the viscosity of the electrolytic solution. Low viscosity electrolytes, which allow high rates of molecular diffusion, also exhibit high vapor pressures and high volatility. Highly volatile electrolytes make device fabrication and sealing extremely difficult, which decreases the shunt resistance and leads to short circuiting and lower current densities [18]. Additionally, the volatile solvent is often able to escape through the cell sealing material. This loss means there is no diffusion of electrolyte and the solar cell ceases to function. In accelerated aging tests at elevated temperatures, this decrease in performance due to solvent loss was found to be the primary concern of dye-sensitized solar cells, where-as dye degradation, iodine loss, and decrease in counter electrode catalytic ability were not [19]. The

improvement of dye-sensitized solar cells is based upon the optimization of each component, in both properties and fabrication, and then the application of each optimized component in a thoroughly optimized dye-sensitized solar cell. New materials must be developed and optimized to further improve upon DSSC functioning.

Solar Cell Substrates and Conductive Coatings

In the attempt to make solar cells as thin and lightweight as possible, flexible plastic substrates have been developed to replace the more commonly used glass slides. When properly modified, new polymer technology may be able to combine the high mechanical strength of conventional polymers with the electrical and optical properties of novel polymers and still make use of easy-to-use mass production extrusion facilities [20]. However, these conductive plastics are difficult to incorporate into the dye-sensitized solar cell design due to the necessity of the high temperature titanium dioxide thermal treatment step (which is discussed in more detail in the next section). With organic solvent electrolytes still dominating the dye solar cell field, polymer films and seals are subject to solvent permeation, eventual solvent loss, and cell stoppage.

The most commonly explored conductive polymer substrate is indium-tin-oxide (ITO) coated poly(ethylene terephtalate). However, the titanium dioxide thermal annealing step is limited to 150 °C due to the degradation of the polymer above this temperature [20]. Poor adhesion and reduced electrical contact have led to new methods of titanium dioxide synthesis and deposition on plastic substrates, either with low temperature annealing or high static pressing [21, 22]. However, neither of these methods achieved results at the level of high temperature annealed TiO_2 cells.

Although glass slides are heavier and brittle, they are easier to work with in the laboratory environment. The slide is coated with a transparent conducting oxide (TCO) film of either ITO or fluorine-doped-tin-oxide (FTO). It is important for thin conductive oxide films to be optically transparent to allow sufficient light penetration for optimal photo-current generation. Thicker layers of conducting oxide enable the glass slide to be more conductive, but too thick of a conductive oxide leads to poor transparency and limits the solar energy passing through the glass for absorption by the dye complex.

ITO coated glass slides have a higher optical transmission than FTO and other investigated TCO coatings [23]. However, it has also been discovered that ITO coating morphology is temperature dependent, both in the initial deposition procedure and especially when subjected to further heat treatment cycles thereafter [24]. At high temperatures, such as the titanium dioxide annealing step in DSSC fabrication, the coating can break down and the cell series resistance may increase substantially. In UND trials, slide resistance increased from 0.26 kΩ to greater than 1.5 kΩ after annealing at 450 °C for thirty minutes. Additionally, it was determined that ITO coatings begin to break down at temperatures greater than 235 °C. Although the slides were of low TCO thickness to begin with, these slides make DSSC fabrication impractical and the achievement of significant results impossible.

FTO coatings have been found to be much more resistant to the heating cycle, as they are able to withstand temperatures in excess of 450 °C, and they are becoming more common in DSSC research because of their thermal stability. Using high TCO thickness FTO slides in UND trials, the cell resistance was found to change from 35 Ω to 50 Ω after heating. This allows the photo-generated current to be fully collected, where as the highly resistant ITO slides in previous trials did not. Higher power conversion efficiencies have been achieved in almost all

instances of FTO over ITO [25]. Only a tri-oxide layer modification utilizing antimony had even higher power conversion efficiencies [26].

Thin Conducting Metal Oxides

Nanocrystalline mesoporous oxide films are the choice material in photoanode fabrication. Inexpensive, optically transparent oxide powder is deposited on the conductive surface of the substrate to form both a high surface area structure for dye adherence and an electrical contact between the conductive substrate surface and the dye particles. The conductive band of the oxide powder accepts photon-excited state electrons from the HOMO level of the dye complex and shuttles those electrons out of the cell as external current to power devices. The particle size, structural morphology, and deposition technique are of utmost importance in the thin conductive oxide film fabrication.

Due to its high abundance, non-toxicity, and low cost, anatase titania (TiO_2) has been by far the most common nanocrystalline oxide utilized in DSSC, but ZnO, SnO_2, Nb_2O_5, and others have also been used [11]. Through doctor-blading, spin-coating, or screen-printing, a sol-gel or paste is deposited on the conductive substrate and heated at high temperatures to create electrically connected mesoporous networks. High surface area films increase light harvesting ability by increasing dye adsorption, but they can also increase recombination and dark current between the oxide conduction band and the electrolytic solution simply because of the greater amount of surface interactions between the oxide, dye, and electrolyte [11]. Sophisticated device architecture is leading towards multi-layered oxide fabrication techniques to inhibit recombination effects by imposing an insulating layer against electron backflow.

Core-shell nanoparticles can be generated by coating a metallic oxide, such as TiO_2, with another, such as zinc oxide (ZnO). This method has led to improved power conversion

efficiencies due to zinc oxide having a higher electronic mobility and carrier lifetime, which decreases recombination mechanisms while exhibiting a similar electron injection step to that of TiO_2 films [27]. Additionally, the effects of several variables were examined with regards to the efficiency of electron injection. The presence of iodide/tri-iodide, and the pH of the TiO_2 preparation were found to have no effect, while the application of an external voltage to orient particle direction showed only weak effects [28].

The most convenient method of achieving higher photocurrents is accomplished by inducing a "light trapping effect" which is done through a muti-layered titanium dioxide fabrication technique [29]. Specific layers of different sized titanium dioxide nanoparticles are deposited in sequence, with each layer performing a specific task. These layers are referred to as a compact "transparent nanocrystalline layer", a light absorbing layer, and a "light scattering layer" [29, 30]. The transparent nanocrystalline layer is composed of <10 nanometer sized TiO_2 particles which permit full light penetration, have high surface area, and pack so tightly they act as a layer to prevent short circuiting between the electrolyte and conductive coating on the glass slide. The light absorbing layer, composed of 25 nm TiO_2 particles, is the primary layer for dye adherence and light absorption. The light scattering layer is made of large 450 nm diameter TiO_2 particles which act to reflect light into the TiO_2 layers and prevent excess light from penetrating the iodide redox electrolyte. Additional anti-reflecting layers may also be used to promote light capture within the titanium dioxide film. A theoretical model attempts to capture 100% of incident light by developing a fiber-type solar cell that allows light penetration in one direction only, thereby preventing any release of incident solar energy and bringing the efficiency of the solar fiber much higher than other cells [31].

Other deposition techniques include electrodeposition, electrospinning, and magnetic sputtering, but it is important to consider industrialization when developing new fabrication

techniques [29]. High vacuum, clean room environments are much more expensive than sol-gel screen-printing, and in an effort to keep the cost of these solar devices low, simple deposition techniques must be optimized. Ideally, existing equipment in roll-to-roll manufacturing could be adapted to suit the needs of this developing industry, whether by using a casting, spin coating, blading, jet-printing, pad-printing, spray coating, or any other type of fabrication process [32, 33]. Roll-to-roll processing is an inexpensive method of achieving high production volumes of thin plastics by depositing materials on sheets of polymeric material as the sheets are unwound from one roll and rewound to another. At this time, only a few companies have been able to achieve the power output necessary to make large scale processing of thin film solar polymer products a feasible economic endeavor.

Very few published results have attempted to make large surface area dye-sensitized solar cells because it seems that at this time, it is more important to achieve high power conversion efficiencies (which exclusively have small surface areas, often less than 0.5 cm^2). Only two records were found for relatively large dye-sensitized solar cells. These were produced by the Energy Research Centre of the Netherlands and the Institute of Photovoltaic, Germany, and achieved 4.7% (2003) and 6.8% (2000) power conversion efficiencies, respectively, and had cell surface areas of 400 cm^2 [11].

Nanoparticle orientation is also proving to be important in device performance. The application of an external voltage bias has been used to orient nanorods perpendicular to the substrate surface, but the significance of this technique has been subject to question after mixed results were reported. However, nanowire arrays developed from a hydrothermal deposition method showed a 17% performance increase over traditional commercial TiO_2 doctor-blading application results [34]. These advancements in nanoparticle structure and orientation are demonstrating a critical improvement in device performance.

Light Harvesting – Sensitizing Dyes and Conjugated Polymers

Once the mesoporous thin conducting oxide layer has been deposited and thermally treated, the particle surface area is coated with an energy absorbing dye by soaking the oxide film in dye solution for approximately twenty hours. Ethanol is a commonly used solvent for the dye, simply because the low boiling point makes ethanol easy to remove from the oxide structure. It also deprotonates the carboxylic acid functional groups on the dye to then allow physical bonding of the dye to the TiO_2 surface.

The ability of colored dye species to absorb light energy is useful in solar concepts, but the dye must also be able to generate and transport excited electrons to the conductive band of the thin conducting oxide layer. Good adhesion to the oxide surface is critical in achieving high electron injection, and the dye should absorb all solar energy below 920 nm to provide sufficient spectral coverage and energy transmittance [11]. In addition, the oxidized dye must be stable enough to hold its oxidized state until it is reduced to its original state by an electrolyte electron, not a recombinatorial electron from the nanoparticulate conductive oxide. These dyes must then be readily restored to their initial electronic state and survive approximately 10^8 reduction-oxidation cycles over the theoretically desired twenty year dye-sensitized solar cell lifetime.

Dye-sensitized solar cells have explored many types of colored complexes, including naturally occurring berry and plant dyes, chemical indicators, light-absorbing polymers, and inorganic metal complexes [35, 36, 37, 38]. The most commonly used dye is a ruthenium polypyridine complex known as N719, or the "Black Dye", and is specifically named di-tetrabutylammonium *cis*-bis(isothiocyanato)bis(2,2'-bipyridyl-4,4'-dicarboxylato)ruthenium(II).

N719 readily absorbs photons across a wide range of the solar spectra (but not the infrared and red regions), easily generates photo-excited electrons to the conducting oxide, and has demonstrated longevity in accelerated lifetime trials [6]. However, because ruthenium exists

in limited supply and is relatively expensive compared to other cell components, common natural dyes found in fruits (i.e. blueberry, raspberry, blackberry) and flowers (i.e. marigolds, violets, rose, lily, et. al.) have been examined [35, 39]. These natural dyes are cheap and convenient, but yield a photocurrent significantly lower than the current produced by N719.

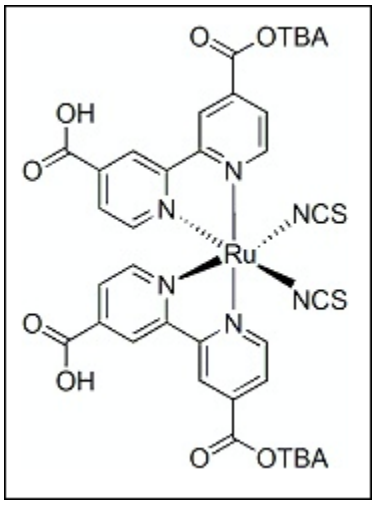

Figure 2. N719 'Black Dye' Structure [11]

An anthocyanine dye extracted from blackberries registered only a 308 μA short circuit current and achieved only 0.33% power conversion efficiency [39]. Other dyes are being developed, but the cost factor of the sensitizing ruthenium dyes, currently priced at about one dollar per milligram, cannot be overlooked. Specifically tailored polymeric materials may work into this niche, as one solar absorbing polymer was first shown to give higher power conversion efficiencies than the comparative N719 dye solar cell in 2009 [37]. Limited novel attempts are being made at making non-ruthenium metal complexes, but much work must still be done.

However, additional research is being done with hybridized cells and tandem cells, which utilize different spectral absorbing components to cover a wider range of the solar spectrum. For example, a hybrid dye-sensitized solar cell using two dyes, one dye to absorb short wavelengths of light and one dye to absorb long wavelengths of light, was found to

harvest light and generate charge comparable to other single dye solar cells absorbing over the same range [40]. Although this may not provide an advantage in this situation, it demonstrates the ability of co-sensitized dyes to work as non-competing complements to increase power conversion efficiency.

Electrolytes –Redox Reagents, Organic Solvents, Ionic Liquids, and Polymers

The electrolytic redox reagent is responsible for restoring the oxidized dye to its original state by replacing the electron lost to the TiO_2. In the process, the reducing agent is converted to an oxidized product and then diffuses through the electrolytic solvent to the counter electrode, where it is regenerated back to the initial reactant state.

By far, the most common redox reagent is a solution of iodide (I^-) and tri-iodide (I_3^-) in acetonitrile. This redox couple has sufficient redox potential energy to quickly regenerate the oxidized dye and also has high diffusion coefficients for both species, especially in volatile organic solvents. The iodide – tri-iodide solution concentration has been studied extensively, and generally is made as a 0.50 M iodide solution and a 0.05 M tri-iodide solution to achieve a 10:1 molar ratio [41, 42]. Cation effects of dissolved iodide solids have also been studied. It was found that as the cation radius increased (from lithium, to sodium, potassium, rubidium, and cesium), the photocurrent decreased and the photovoltage increased due to the formation of a cationic inhibition layer on the TiO_2 surface [43]. Since high photocurrent is desired, typical redox electrolytes now employ lithium iodide as the reducing reagent. Additives, such as 4-*tert*-butylpyridine and guanidinium thiocyanate are commonly used in the electrolyte to inhibit specific recombination mechanisms between the excited state electrons and redox reagent [37, 39]. The amount of 4-*tert*-butylpyridine (the most common additive) has been optimized at 0.5 M in the electrolyte [44]. These additives work by binding to active TiO_2 sites and blocking exciton-

iodide recombination reactions. This benefits the cell by decreasing the amount of adsorbed protons and/or Li^+ ions on the titanium dioxide surface, which results in higher electron flow and decreases the recombination of electrons in the titanium dioxide with tri-iodide in the electrolyte [44]. This shift in electron injection dynamics is strongly correlated with a shift of the TiO_2 conduction band. Specifically, a 100 meV shift results in up to a doubling of electron injection retardation [28]. Optimization of these additives and the concentrations of all necessary components is only a first step in electrolyte preparation. New electrolytes with both higher stabilities and higher ionic conductivities are now being sought after, and ionic liquids have proven to work into this niche quite well.

Ionic liquids are classified as any ionic compound with a melting point below 100 °C, but room temperature ionic liquids (that are actually in liquid state) are most commonly used in this branch of dye solar cell research [45]. The ability to remain in liquid state at such low temperatures is due to the large, asymmetric structures of these molecules which decrease lattice energy and delocalize charge. Ionic liquids generally have interesting properties which are very useful for dye-sensitized solar cell electrolytes, including high thermal stability, moderate viscosity (<100 cp), good ionic conductivity, excellent solvating abilities, and negligible vapor pressure [46]. Several forms of ionic liquids have been used to create mixtures, composites, and gels with varying degrees of these desired properties. Examples of the ionic liquids used in these studies include several various forms of cationic imidazolium, ammonium, pyridinium, pyrrolidinium, phosphonium, and sulfonium [37, 46, 47, 48, 49, 50, 51]. Some common ionic liquid cations are shown in Figure 3. Properties can also be manipulated based on the fact that ionic liquid cation type generally affects the conductivity and viscosity of the ionic liquid, while anion type is more closely correlated to chemical reactivity. In particular, imidazolium species have been shown to demonstrate high thermal stabilities, excellent ionic conductivities, and high densities [52, 53].

Additional additives, used to increase the viscosity of the electrolyte, have included poly(vinylideneflouride), polyethylene oxide, polyaniline-loaded carbon black, and carbon nanotubes [47, 48, 49, 50]. This increase in viscosity was able to increase cell stability and lifetime, but at the cost of lowering ionic diffusion and cell performance. Solid-state, all polymer electrolytes based on poly(ethylene oxide) have demonstrated a power conversion efficiency of 2.0%, but the low ionic diffusion and low penetration of polymer electrolyte into the titanium dioxide electrode limit the achievable current [54]. Using a polymer as an additive is proving to be a much more practical solution in decreasing the electrolyte volatility while maintaining high ionic conductivity. These studies have been attempted while controlling a variety of parameters which affect the viscosity and the conductivity, including polymer concentration, polymer type, iodide salt concentration and type, alkyl chain length, and organic solvent content [55].

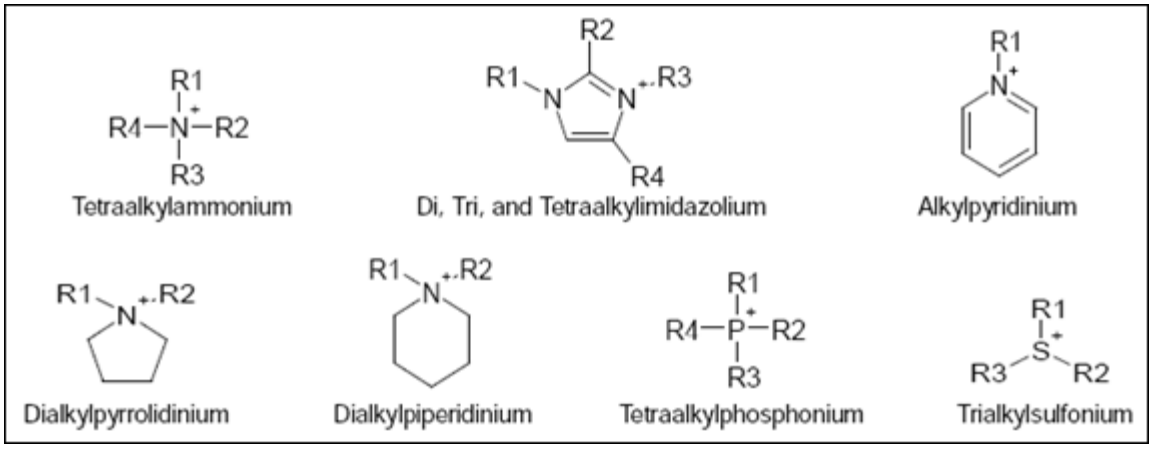

Figure 3. Common Cations of Ionic Liquids for Electrochemical Applications [44]

The creation of quasi-solid state electrolytes is becoming a prominent research field for dye-sensitized solar cells. Some of these quasi-solid state electrolytes include solvent swelled polymer networks, polymeric gels, plasticized polymers, or polyelectrolytes [36, 56, 57, 58, 59, 60, 61]. Polymeric gels are swollen polymeric networks, whereas plasticized electrolytes are polymers which have been swollen with small amounts of plasticizer, often a low molar mass polyether [20].

Polyelectrolytes are ionic polymers in which charge is attached to the polymer and ionic transfer properties are attributed to the mobility of the counter ions, which have dissociated from the polymer functional groups.

These gels or swelled polymers have demonstrated the increased stability and high conductivity many research teams have been looking for. Gelators and ionic liquids were used to create highly stable quasi-solid state polymer electrolytes from poly(vinylidenefluoride-co-hexaflouropropylene) [56]. Although the diffusion of the electrolyte is still considered "good", the power conversion efficiencies of the cell dropped to around 6% depending on the weight percent of imidazolium based ionic liquid and polyacrylonitrile used in the gelation. In another study, using ethanol instead of water as a solvent was found to increase the power conversion efficiency of a poly(ethylene oxide)-poly(vinylidene fluoride) gel electrolyte [57]. Permanent thermosetting gel electrolytes were produced from poly(acrylic acid)-(ethylene glycol) and optimized to generate power conversion efficiencies around 6% [36]. A second thermosetting polymer gel was made with oligomeric ethylene glycol and polyvinyl pyrrolidone to produce quasi-solid state dye-sensitized solar cells with power conversion efficiencies around 2.4% [58]. However, the trade-off between stability and efficiency is still apparent in some trials. The performance of quasi-solid state electrolyte dye-sensitized solar cells is always lower than those containing liquid electrolytes [56]. A solid poly(vinylpyridine) derivative was doped with varying weight percents of ionic liquid to form solid-state electrolytes and these cells achieved at most 0.65% power conversion efficiency [59].

Advanced ionic liquid applications in polymer science have led to exotic polymerized ionic liquid polyelectrolytes, ionic liquid plasticizers, and porous polymer materials [60]. The modifications in many of these projects do not significantly change ionic conductivity and are therefore very exciting for electrolytic materials research. Gorlov and Kloo report a thorough

summary of dye-sensitized solar cells using ionic liquids as liquid electrolytes and in quasi-solid electrolytes; the highest ionic liquid electrolyte power conversion efficiency of 8.0% used 1-propyl-3-methylimidazolium iodide and N-methylbenzimidazole, while the highest quasi-solid electrolyte power conversion efficiency of 7.1% used 1-ethyl-3-methylimidazolium iodide and poly(ethylene glycol) [61].

The diffusion of the iodide and tri-iodide throughout the electrolytic material has also been a topic of much interest. Since tri-iodide is a larger molecular species, its diffusion coefficient is generally more of a concern and is looked at in more detail than that of iodide. High diffusion is desired to make redox agents readily available in the cell regeneration cycle, but the diffusion is greatly dependent upon the solvent, or non-solvent material, used. In highly volatile organic solvents, diffusion of iodide species are high and cell performance parameters are also high, but they are very short lived due to solvent loss [62]. In low vapor pressure solvents, such as ionic liquids, diffusion is lower, but increased cell stability is achieved. Table 1 summarizes a few selected diffusion coefficients for tri-iodide, and it can be noted that its ability to diffuse decreases by at least an order of magnitude in non-liquid type solvents.

Table 1. Diffusion Coefficients for Tri-iodide [43, 56, 62]

Solvent	ACN, Li^+	CH_3OCH_2CN	PC, TPA^+	PMIMI	PEG, BuPy, Li^+
D / (cm^2 / s)	1.5 $x10^{-5}$	5.4-6.2 $x10^{-6}$	1.9 x 10^{-6}	1.5 $x10^{-7}$	4.5 $x10^{-8}$

ACN, acetonitrile; PC, poly(carbonate); TPA^+, tetrapropyl ammonium; PMIMI, 1-propyl-3-methyl imidazolium iodide; PEG, poly(ethylene glycol); BuPy, 4-*tert*-butyl pyridine

Additionally, the diffusion coefficient is thought by some researchers to be a combination of physical diffusion and a bond exchange Grotthus-type mechanism [41]. Grotthus mechanisms explain how charge transfer of protons occurs so rapidly compared to other ionic molecules. This transfer is a relay of simultaneous bond formation and deformation, which

results in an apparent change of location for a charged species. In fact, it is a different individual molecule which now carries the localized charge. Although Grotthus mechanisms generally refer to proton hopping, the concept can be extended to other ions in highly ionic environments. Depending upon the constraints of the solvent-solute interactions, either mechanism may be dominant. For example, tri-iodide has been shown to demonstrate good diffusion properties in polymer gel electrolytes consisting of polyethylene oxide in propylene carbonate/ethylene carbonate, even with the increased viscosity of the gel due to the polymer network [62, 63, 64]. This variation in diffusion mechanisms led to the hypothesis of an iodide polyelectrolyte promoting conductance through the cell.

Counter Electrodes – Catalytic Metals and Carbon Nanotubes

The counter electrode is deposited on the conductive surface of the rear cell substrate. It facilitates electron exchange from the incoming current to the electrolyte through either a catalytic mechanism or simple electron conduction. Catalytic metals such as silver, platinum, and gold have been used as a counter electrode in high performing dye solar cells. However, these catalytic metals were discovered to facilitate a destructive iodide reaction that eventually leads to cell stoppage [43]. This has led to the development of carbon nanotube films as counter electrodes since they were found not to degrade [65, 66]. It was also noted that ionic liquid-water mixtures have the ability to react when catalyzed by platinum, and the reaction creates a charge inhibitive species layer [67]. This research reveals an additional benefit in developing carbon based electron transfer counter electrodes. Low cost carbonaceous materials such as graphite, acetylene black, and ketjen black, in pure form and as mixtures, were also used for counter electrodes and demonstrated better solar cell output parameters than platinum electrodes, both upon initial cell fabrication and over the course of a cell lifetime [68].

Carbon nanotubes are made of planar carbon rings wrapped in a tubular dimension. Carbon rings and sheets are able to facilitate electron transfer due to the high mobility of electrons within those rings and sheets. Carbon nanotubes are commonly available in single, double, and multiwall varieties, and may exist in two simply described forms: “Russian Doll” or “Scroll.” The Russian doll model is a nanotube within a nanotube (i.e. double walled), while the scroll form would look like a rolled sheet of thin carbon, rolled twice to be two layers thick (i.e. double walled). Multiwall carbon nanotubes are essentially any wall number greater than two.

Single wall carbon nanotubes have been found to be the most transparent variety and are therefore used in cell materials where light penetration is critical, such as when they are used on the photoanode [69, 70]. There are conflicting reports of which nanotube is optimal for counter electrodes in dye-sensitized solar cells. Single wall carbon nanotubes have the highest conductivity, especially when deposited in a manner to align the tubes perpendicular to the substrate. Multiwall carbon nanotubes have higher surface areas with a greater number of defect rich planes which allow for more interfacing of both the electrolyte and the conductive substrate, resulting in better electron transfer [70]. It has also been found that nanotube film electron transfer dynamics can be affected by deposition technique, as well as chemical modifications to the nanotubes using thionyl or ozone treatments [71, 72, 73]. Nanotube diameters have also been reported to be of importance, where large diameter nanotubes (100 ± 10 nm) showed lower reaction resistance and faster response time compared to small diameter nanotubes when regenerating iodide from tri-iodide at the counter electrode surface [74]. Finally, heat treatment cycles may provide an impact in cell performance, as a two step air dry and high temperature bake under nitrogen was shown to increase the interface area between the carbon nanotubes and electrolyte, which therefore increased effective iodine diffusion [75].

Summary

A few final DSSC examples help show the wide variety of combinations of materials discussed in the preceding sections. First, an ionic liquid gel was irradiated to form a solid state electrolyte [76]. Carbon nanotubes were used as conductive films on both the top and counter electrode substrate surfaces, which were flexible polyethylene terephthalate (not glass slides). Zinc oxide nanoparticles were dispersed on the top carbon nanotube film. Very low power conversion efficiencies were achieved, but the concept did work. A second project polymerized an ionic liquid to create a solid state electrolyte, which was used in conjunction with conductive polymers poly(3,4-ethylenedioxithiophene)/poly(styrenesulfonate) on carbon nanotube, FTO coated glass slides [77]. A power conversion efficiency of 3.7% was reported.

A recent report by Gratzel, et.al., not only shows the extent of dye-sensitized solar cell technology, but also demonstrates just how much is still unknown about potential cell materials and design. The new cell fabricated in his laboratories has achieved the highest DSSC conversion efficiency to date of 12.3% and did so while reaching two important objectives which will change the direction of future research [10]. This cell has found replacements for both the problematic iodide – tri-iodide electrolyte species and the expensive ruthenium dye. Instead, the cell uses a cobalt II/III redox agent in conjunction with a custom synthesized zinc porphyrin dye and co-sensitizer. The ability of a cell to operate without the thought-to-be-critical dye and electrolyte core components is a huge breakthrough in this field, not only because of the avoidance of the problematic materials, but also due to the highest yet reported power conversion efficiency. The reported PCE is now high enough to compete with other solar markets and future research can now focus on bringing this device to the large scale.

Finally, the concept of tandem dye-sensitized solar cells has been explored as a way to increase current using similar cells stacked on each other and/or using different solar absorbing

complexes. An increase in both short circuit current density and open circuit voltage resulted in power conversion efficiencies over ten percent, despite a very low fill factor [79, 80]. Perhaps other cells, in tandem with the breakthrough Gratzel cell, can achieve even higher power output in the not-too-distant future.

In conclusion, the research and development of dye-sensitized solar cell materials and fabrication processes is extremely diverse. A very simple illustration of this diversity can be found in Table 2, which summarizes only a small sample of the wide variety of dye-sensitized solar cells being looked into. Additionally, these cells tend to be optimized for specific sets of components only. Exchanging one part leads to entirely new results and it is often difficult to decipher which effect is most important. The lack of statistical significance in reports is rather disappointing, but hopefully as specific cell materials become more main stream, an optimized method of fabrication may lead to better methods of data interpretation and reporting.

Table 2. Selected DSSC to Demonstrate Variety of Concepts and Results (Tested at 1000 W/m^2)

DSSC Cell Novelty	PCE / %	V_{oc} / V	J_{sc} / (mA/cm^2)	Area / cm^2	FF / %	Date	Reference
Original DSSC by Gratzel & O'Regan	7.1	0.68	12	0.5	68	1991	Gratzel & O'Regan [5]
Conducting plastic substrate	2.3	0.76	7.3	0.32	41	2001	Lindstrom, *et.al.* [21]
Gelated electrolyte using amide/urethane	5.9	0.67	12.8	--	--	2001	Kuba, *et.al*. [19]
MPII combined with PVDF-HFP polymer gel electrolyte	5.3	0.665	11.29	0.152	71.2	2002	Wang, *et.al.* [46]
Gel polymer electrolyte using acrylonitrile-methyl methacrylate	2.4	0.72	6.27	0.25	53	2005	Kim, *et.al.* [61]
NREL Verified Record DSSC by Sharp Corp.	10.4	0.729	22	1.004	65.2	2005	Green, *et.al*. [6]
Thermosetting gel electrolyte using poly(acrylic acid)-(ethylene glycol) hybrid	6.1	0.735	12.55	0.2	66.1	2007	Wu, *et.al.* [36]
ITO/ATO/TiO_2 conducting oxide layer	6.41	0.813	10.74	0.281	73.4	2008	Yoo, *et.al*. [25]
$TiCl_4$ pre-treatment, electrolyte of BMII, I_2, GuNCS, tBP, acetonitrile/valeronitrile	10.1	0.789	18.2	0.25	70.4	2008	Ito, *et.al.* [28]
Solvent free Ionic Liquid electroltye	8.2	0.741	14.26	--	77.4	2008	Bai, *et.al.* [48]
Full solid state, flexible, novel ionic liquid gel, organic dye, ZnO and CNT films on PET substrate for possible roll-to-roll process	--	0.23	2.23	--	--	2008	Wei, *et.al.* [73]
MWCNT used as counter electrode	7.67	0.74	16.2	0.36	64	2009	Lee, et.al. [69]
Series connected tandem DSSC	10.4	1.45	10.8	0.25	67	2009	Yamaguchi, *et.al.* [77]
MWCNT added to electrolyte	4.36	0.69	10.55	--	61	2010	Lee, *et.al.* [64]
EMIMDCN doped PVPI solid polymer electrolyte	0.65	0.7	3.04	0.25	30.7	2010	Singh, *et.al.* [58]
Polymerized IL electrolyte and SWCNT gel	3.7	0.7	9	--	58	2010	Kawano, *et.al.* [76]
Polyene-diphenylaniline organic dye, electrolyte of ionic liquids PMII and $EMIB(CN)_4$	6.5	0.714	12.4	0.158	73	2011	Kuang, *et.al.* [38]
Natural dye extracted from violets	0.33	0.498	1.02	--	64.5	2011	Zhou, *et.al.* [33]
Porphyrin – organic dye co-sensitizer, Co(II/III) electrolyte	12.3	0.935	17.66	--	74	2012	Gratzel [10]

PCE, power conversion efficiency; V_{oc}, open circuit voltage; J_{sc}, short circuit current density; FF, fill factor

CHAPTER III

HYPOTHESIS & EXPERIMENTAL DESIGN

Poly(diallyldimethylammonium iodide), poly(DADMAI), will be obtained from poly(diallyldimethylammonium chloride), poly(DADMAC). This new polymer electrolyte may allow the necessary charge transport in the polymer membrane to occur via a combined effect of the charged polyelectrolyte polymer structure and the availability of the additional iodide ions in poly(DADMAI). The additional iodide ions may also promote cell stability by providing a long lasting supply of iodide in the event of iodide-degrading side reactions. Therefore, it is hypothesized that by swelling the novel polyelectrolyte with ionic liquid solvent, a highly conductive and long lasting electrolyte can be produced for use in dye-sensitized solar cells. Although this concept has been attempted using other polymeric materials, this combination has yet to be attempted and it may provide a novel method of bringing together the desired goal of both the high performance of low viscosity electrolytes and the high stability of solid-state electrolytes.

The full factorial experimental design (Table 3, next page) investigated the significance of the polyelectrolyte molecular weight, the effect of poly(DADMAC) vs. poly(DADMAI), ionic liquid (IL) alkyl chain length (specifically 1-butyl-3-methyl imidazolium iodide compared to 1-hexyl-3-methyl imidazolium iodide), and the loading ratio of ionic liquid to polyelectrolyte.

This design first investigated poly(DADMAC) molecular weight, ionic liquid type, and ionic liquid weight percent, or 2^3 total runs. Four replicates were performed, for a total of

thirty-two solar cells, to lower variance in similar cell trials. Significant effects were determined by the difference of cell averages at high and low values for each variable, and the design was simplified for poly(DADMAI) by removing the ionic liquid to polyelectrolyte loading ratio variable once it was deemed insignificant. Cells were constructed for poly(DADMAI) molecular weight and ionic liquid type trials, or 2^2 total runs, and performed in four replicates for a total of 16 solar cells. A full list of experimental trials is summarized in Table 4.

In addition, average dye-sensitized solar cell parameters were determined using a standard electrolyte in acetonitrile solution. These averages were used as a baseline for comparison of the results of this study. Cells using electrolytes of pure ionic liquids were also fabricated for comparison.

Table 3. Full Factorial Experimental Design Variables

Variable	Low (-1)	High (+1)
Polymer MW / (g/mol)	<100,000	400,000 – 500,000
Polymer Type	poly(DADMAC)	poly(DADMAI)
Ionic Liquid	butyl Im-I	hexyl Im-I
wt % IL	50%	75%

Table 4. Experimental Design Trials

Polymer Type	Polymer MW (g/mol)	Ionic Liquid	wt % IL	Replicates
poly(DADMAC)	-1	-1	-1	4
poly(DADMAC)	-1	-1	+1	4
poly(DADMAC)	-1	+1	-1	4
poly(DADMAC)	-1	+1	+1	4
poly(DADMAC)	+1	-1	-1	4
poly(DADMAC)	+1	-1	+1	4
poly(DADMAC)	+1	+1	-1	4
poly(DADMAC)	+1	+1	+1	4
poly(DADMAI)	-1	-1	--	4
poly(DADMAI)	-1	+1	--	4
poly(DADMAI)	+1	-1	--	4
poly(DADMAI)	+1	+1	--	4

CHAPTER IV

CHEMICALS, MATERIALS, & EQUIPMENT

Materials were used as received unless otherwise noted. Solvents used were laboratory grade unless otherwise noted. All water used in any procedure was distilled and de-ionized.

Indium-tin-oxide glass slides (70-100 Ω/square) were purchased from Delta Technologies, Ltd. Flourine-doped-tin-oxide slides were purchased from Hartford Glass Company (USA). Slide conductivity was verified using a Keithley 2420 sourcemeter. Methanol and acetone were used, respectively, to clean the surface of the slides prior to titanium dioxide and carbon nanotube deposition.

Compact layer titanium dioxide (four nanometer diameter) was synthesized from titanium isopropoxide purchased from Sigma Aldrich. Degussa P25 titanium dioxide (twenty-five nanometer average diameter) was used as the light absorbing layer. Light scattering 99.8% titanium dioxide anatase (four hundred fifty nanometer diameter), Lot# MKBG3671V, was purchased from Sigma Aldrich. Water and Triton X-100 were weighed on a Denver Instruments digital analytical balance (model APX-200) and added to the titanium dioxide in a small sealable glass vial. The mixture was homogenously dispersed by both the Vortex Genie 2, model G-560 from Scientific Industries, Inc., and by sonication of the vial in a Fischer Scientific Ultrasonic Cleaner, model FS60H, to produce sol-gels for titanium dioxide deposition.

Titanium dioxide pastes were dropcast using variable volume 250 µL transferpettes and then spun using an SCK-100 spin coater from Instras Scientific LLC. A piece of blue laboratory tape (Sigma Aldrich) with a hole punched out (using a common hole punch) was used as the casting template. The post treatment titanium isopropoxide was diluted using isopropanol. A Vulcan 3-550 digital furnace was used to heat the titanium dioxide depositions.

Di-tetrabutylammonium *cis*-bis(isothiocyanato)bis(2,2'-bipyridyl-4,4'-dicarboxylato)ruthenium(II) was dissolved in absolute ethanol. The storage flask was wrapped in aluminum foil to prevent excess exposure to light before use.

Multi-wall carbon nanotubes from Sigma Aldrich (outer diameter 20-40 nanometers, inner diameter 5-10 nanometers, length 0.5 – 50 micrometers, purity >95%) were mixed with carboxymethylcellulose sodium salt from Fluka (purum, ultra high viscosity 1500 – 4500 mPa·s), and distilled, de-ionized water to form carbon nanotube sol-gel paste for the counter electrode deposition. This paste was doctor-bladed with a glass stir rod on the rear slide using blue laboratory tape as a thickness template. The paste was heated in the same oven as the titanium dioxide sol-gels.

The cells were assembled and glued together using Instant Krazy® Glue ("no run" gel variety). Parafilm® spacers were specifically cut as a spacer template using scissors, a hole punch, and an X-ACTO® knife. Channels were sealed with two part epoxy DP-100 3M Scotch-Weld®.

The electrolytes were prepared using 99.9% lithium iodide, 98.5% 1-hexyl-3-methylimidazolium iodide, and 98.5% 1-butyl-3-methylimidazolium iodide, all from Sigma Aldrich. Laboratory grade resublimed solid iodine, I35-500, from Fisher Scientific was added to generate tri-iodide ions in the electrolyte. Poly(diallyldimethylammonium chloride) was also purchased from Sigma Aldrich, in both <100,000 g/mol (35 wt%) and 400,000 – 500,000 g/mol

(20 wt%) average molecular weight solutions in water. Potassium iodide from Sigma Aldrich, 99% purity, batch# 07208D8, was used to synthesize poly(diallyldimethylammonium iodide) from the chlorinated polymer solution. Poly(diallyldimethylammonium iodide) was characterized using a PerkinElmer Jade Differential Scanning Calorimeter to determine glass transition and melting temperatures, a Hitachi S-3400N Scanning Electron Microscope to observe surface characteristics, and an X-ray fluorescence spectrometer by IXRF Systems, Inc. (which used EDS2008 (version 1.1 Rev C) Energy Dispersion Spectroscopy) for compositional analysis by element.

Fabricated dye-sensitized solar cells were illuminated using a xenon arc lamp in a model LS1000 solar simulator, powered by an XPS1000 Xenon Lamp Power Supply, by Solar Light Company (USA). The light output was standardized to an intensity of 1000 watts per square meter using Solar Light Company's PMA 2100 data-logging radiometer and a PMA2144 Class II pyranometer. The voltage sweep was conducted using the Keithley 2420 source meter and the data was collected using LabTracer 2.0 software. Data analysis was performed in Microsoft Office Excel 2007 and Minitab 15.

CHAPTER V

SOLAR CELL FABRICATION PROCEDURE

Standard Dye-Sensitized Solar Cell Fabrication Procedure

The procedure used for dye-sensitized solar cell fabrication is a modified version of the procedure developed at South Dakota State University by Curtiss Kovash, Jr. under the direction of Dr. Brian Logue [30].

Titanium Dioxide Nanoparticle and Sol-gel Synthesis

The titanium dioxide layer was composed of three distinct layers of differing nanoparticle size. Each particle size, (four nanometer, twenty-five nanometer, and four-hundred-fifty nanometer average diameters), was dispersed as a sol-gel and used to deposit the compact layer, paste layer, and light scattering layer, respectively. The compact layer nanoparticles were developed using nitric acid and titanium isopropoxide. The dry, white powder was collected in a mortar and ground into a fine, consistent powder with a pestle. It was then placed into a vial for compact layer sol-gel preparation. Titanium dioxide prepared in this manner has an average particle diameter of four nanometers [30].

The compact titanium dioxide layer sol-gel was prepared by addition of 0.5 g of the four nanometer titanium dioxide to 2.0 g of de-ionized water in a small vial. An addition of 0.03 g of Triton X-100 (a non-ionic surfactant to help deter particle aggregation) was followed by mixing with the Vortex Genie to disperse the oxide. The vial was then sonicated for thirty minutes until

the titanium dioxide was homogenously dispersed. The paste layer was produced using 0.3 g of Degussa P25 nanoparticles (average particle size twenty five nanometers), which were placed in a small vial. An addition of 1.25 g de-ionized water and 0.015 g of Triton X-100 were added. The mixture was dispersed using the Vortex Genie and then sonicated for thirty minutes to ensure a homogenous dispersion.

The light scattering layer was produced using 0.3 g of Sigma Aldrich titanium dioxide nanoparticles (average particle size four hundred fifty nanometers), which were placed in a small vial. An addition of 1.25 g de-ionized water and 0.015 g of Triton X-100 were added. The mixture was dispersed using the Vortex Genie and then sonicated for thirty minutes to ensure a homogenous dispersion.

The post-treatment solution was prepared from 20 mL of isopropanol placed in a small vial. An adjustable pipette was used to measure 296 µL of titanium isopropoxide, which was then injected into the isopropanol.

Titanium Dioxide Film Deposition Technique and Procedure

A glass scribe was used to cut each glass slide into two 1.5 cm x 2.5 cm rectangles. The conductive side of the glass slides was determined using the Keithley source meter. Using two sided Scotch® tape, the slide was taped on the spin coater with the conductive side up (see Figure 4). The slide was spun at approximately 2500 – 3000 rpm and sprayed with methanol, methanol and acetone, and then only acetone to clean the slide.

A circular hole was punched out (area determined to be 0.2750 cm^2) of a piece of blue laboratory tape using a common hole punch. The tape was firmly pressed down over the conductive surface of the glass slide to act as a template for the titanium dioxide deposition (refer to Figure 5). The tape template was determined to be approximately 50 µm thick.

With the slide not spinning, just enough compact layer titanium dioxide sol-gel was deposited, using a handheld transfer pipette, to cover the template hole. The slide was spun for five seconds at about 2500 rpm to remove excess sol-gel. This layer is very thin, so it is not observable to the naked eye. However, it was observed that the refractive index changed due to the coating, and the slide became more transparent. This deposition procedure was repeated twice more for this slide.

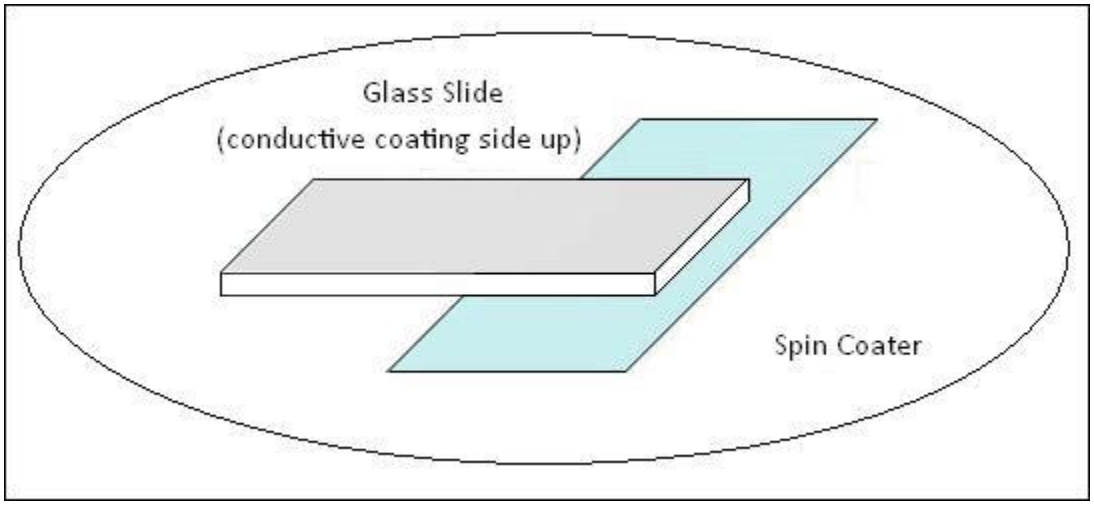

Figure 4. Taping Template for Cleaning Glass Slide

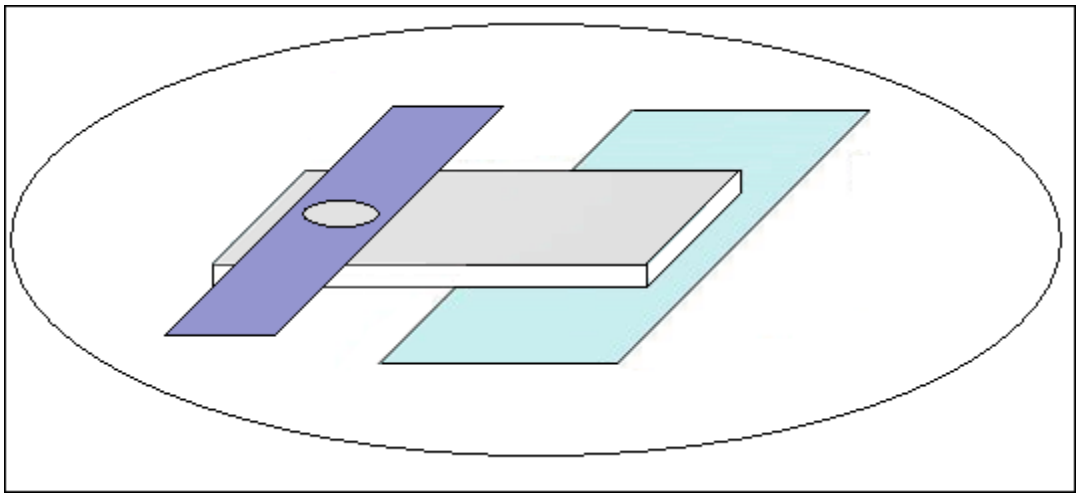

Figure 5. Taping Template for Titanium Dioxide Deposition

The compact layer titanium dioxide was heated in the furnace at 95 °C for five minutes, 225 °C for ten minutes, and 450 °C for thirty minutes. A temperature ramp rate of 40 °C/min was used.

Once the compact layer was thermally treated and cooled, the same tape template was re-applied to the glass slide on the spin coater. Care was taken when re-applying the tape to ensure the compact layer was completely exposed and the remaining surface of the glass slide was completely covered. The previously described deposition procedure was used to apply the Degussa paste titanium dioxide sol-gel. After the third dropcast, the slide was removed from the spin coater and allowed to air dry for a few minutes. The tape template was removed and the slide heated at 225 °C for ten minutes. Once the slide cooled, the same tape template was re-applied and another Degussa paste layer of titanium dioxide was deposited, using the same procedure. The Degussa paste layer deposition procedure and subsequent heating were repeated as described until five layers of titanium dioxide paste had been independently deposited and heated. Each application cycle deposits 8-10 μm of TiO_2, so the final thickness is approximately the same thickness as the tape template. On the fifth thermal treatment, the slide was heated using the 95 °C (five minutes), 225 °C (ten minutes), and 450 °C (thirty minutes) heating cycle.

Once the fifth Degussa paste layer had been heated and cooled, the blue tape template was re-applied. A transfer pipette was used to apply just enough light scattering layer titanium dioxide to cover the template hole and the slide was spun for five seconds at 2500 rpm. This was repeated twice more using the light scattering layer of titanium dioxide. On the third dropcast, the slide was spun for eight to ten seconds at 3000 rpm to ensure uniform deposition and removal of excess sol-gel. The slide was removed from the spin coater and allowed to air dry for

a few minutes. The tape was removed and the slide heated at 95 °C for five minutes, 225 °C for ten minutes, and 450 °C for thirty minutes.

Inside of an overturned 1 L beaker, a small beaker of water was heated to boiling for a few minutes to create a water-saturated environment. Once the slides were removed from the oven and cooled, the white circular titanium dioxide depositions and the surrounding exposed surface of the slide were coated with titanium isopropoxide post-treatment solution and spun for five seconds at 2500 rpm (Figure 6). This was repeated twice. Once the third coating was spun, the slide was removed from the spin coater. The slides were quickly placed onto the hotplate underneath the overturned 1 L beaker in the water saturated environment. After thirty minutes, the slides were removed, rinsed with de-ionized water, and heated at 450 °C for fifteen minutes in the furnace.

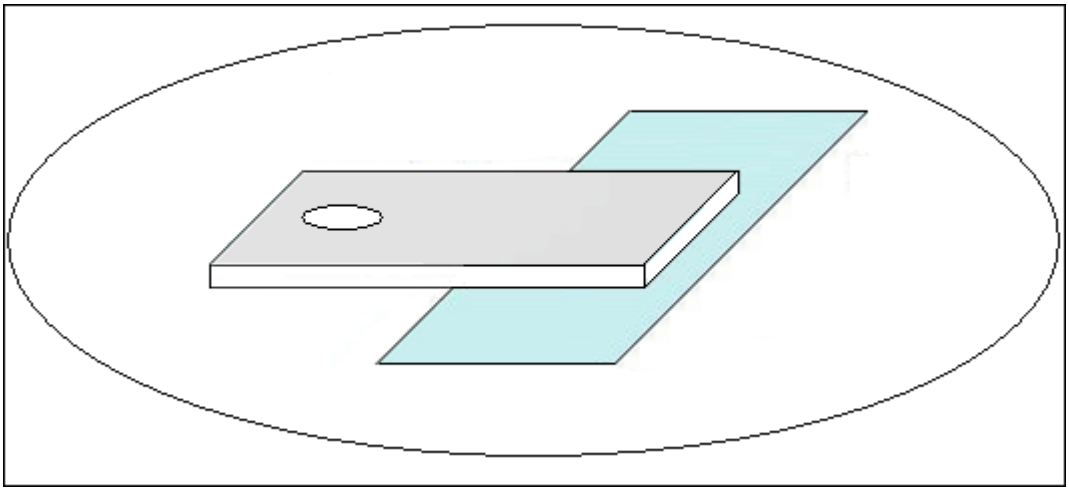

Figure 6. Taping Template for Post-Treatment Step

Application of the Ruthenium Dye Complex

The N719 ruthenium dye is slightly air sensitive and light sensitive, so care was taken to minimize exposure to light and air. In a 10.00 mL volumetric flask, absolute ethanol and 0.0059 g of dye were added to prepare a 0.5 mM solution.

The dye solution was placed on a hotplate and warmed to 70 °C. When the slides finished in the oven, they were cooled to approximately 70 °C and placed into the warm dye solution. The titanium dioxide layers were completely submerged in the dye solution before being removed from the hotplate. The dye was allowed to adsorb onto the titanium dioxide for a minimum of twenty four hours. Any additional time spent in the dye solution does not help or deter the cell in any way, so it is acceptable to leave the cell in the solution for even longer [30].

Once the dye had adsorbed for twenty four hours, the slides were removed and gently rinsed with absolute ethanol. The dyed titania was a dark rose-purple color. The slides were used in dye-solar cell production immediately.

Preparation of Carbon Nanotube Sol-Gel and Counter Electrode Deposition

The carbon nanotube counter electrode deposition technique was adapted from Lee, et. al., and multi-wall carbon nanotubes were used instead of single-wall carbon nanotubes due the usefulness of defect-rich edge planes which facilitate electron-transfer kinetics in the thin carbon film [69]. Additionally, single-wall carbon nanotubes are more optically transparent, which is not a necessary requirement for counter electrode functionality, due to the fact these nanotubes are on the cell counter electrode and do not inhibit solar absorption. A modified heat treatment procedure was adapted from Kang, Han, Choi, and Jeon, in conjunction with the reports from Lee, et.al., for creating an electronically conductive carbon nanotube film [70, 75].

The carbon nanotube sol-gel was produced using 0.16 g of carboxymethyl cellulose sodium salt dissolved in 19.84 mL of distilled, de-ionized water in an Erlenmeyer flask. To this solution, 2.25 g of multiwall carbon nanotubes were added and the entire mixture was magnetically stirred at high speeds for several days until a homogenous carbon nanotube paste was formed. The final carbon nanotube paste was a smooth, jet-black ink. The paste was

continuously stirred even when not in use, and was sealed with a stopper and Parafilm® at all times.

The carbon nanotube sol-gel was doctor-bladed onto the conductive side of glass slides for use as a counter electrode. It was desired to produce counter electrodes in such a manner that the circular titanium dioxide layer was completely covered by the carbon nanotube counter electrode. First, the conductive side of the slide was washed with methanol, methanol and acetone, and then acetone. Using blue laboratory tape, a hole was punched using the same common hole punch as in the previous template constructions, and a drop of carbon nanotube sol-gel was deposited (refer to Figure 7, below). A glass stir rod was then used to swiftly and smoothly "doctor blade" the sol-gel into a continuous 50 µm thick layer.

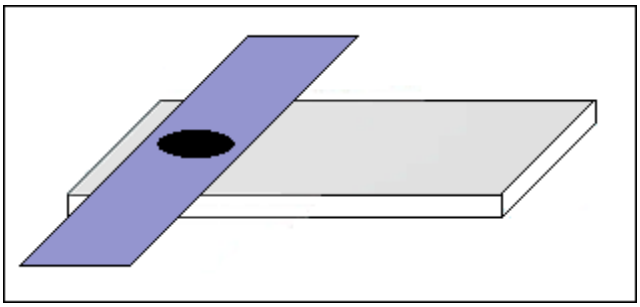

Figure 7. Taping Template for Carbon Nanotube Sol-Gel Deposition

The carbon nanotube film was allowed to dry for a few moments before removing the blue tape template. This film was then baked at 50 °C for three hours in the furnace, followed by heating at 140 °C for thirty minutes.

Preparation of the Electrolyte Spacer and Cell Assembly Procedure

Parafilm® sheets of approximately 75 µm in thickness were cut into 1.5 cm x 1.5 cm squares. Two squares were overlapped to form a spacer two sheets thick and a hole was then punched from the center using a hole punch. Scissors were used to cut narrow channels above

and below the hole, but not centered on one another, to allow full electrolyte penetration. Note that after channel cutting, the spacer is two independent pieces (refer to Figure 8) which were fit together to form a circular cut-out.

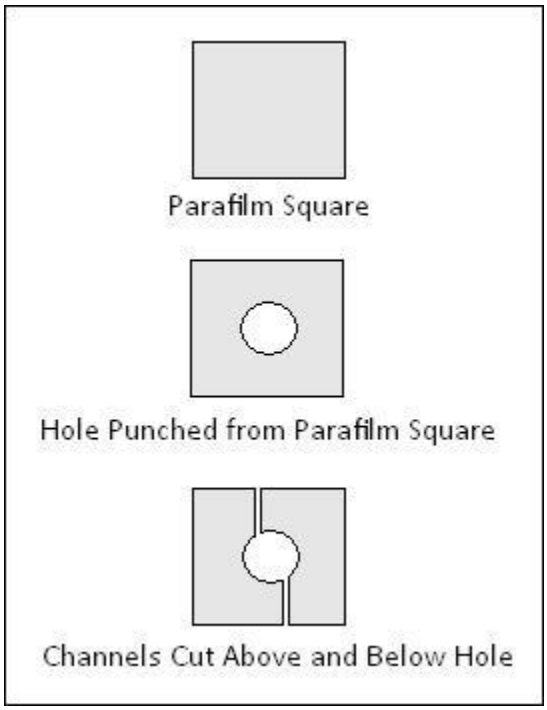

Figure 8. Preparation of Electrolyte Spacer

The spacer was then centered on the circular dye-stained titanium dioxide layer, the carbon nanotube counter electrode was flipped over and sandwiched onto the Parafilm® (see Figure 9, next page), and the cell was heated at 50 °C for a few minutes on a hotplate. This made the Parafilm® slightly waxy so it adhered to the surfaces of the cell. This adhesion is not sufficient to seal the cell completely, but it does hold the slides together while glue is applied around the edges of the cell. The excess Parafilm® was trimmed from the edges of the cell using an XACTO® knife and Krazy® Glue Gel was applied around the edges of the cell.

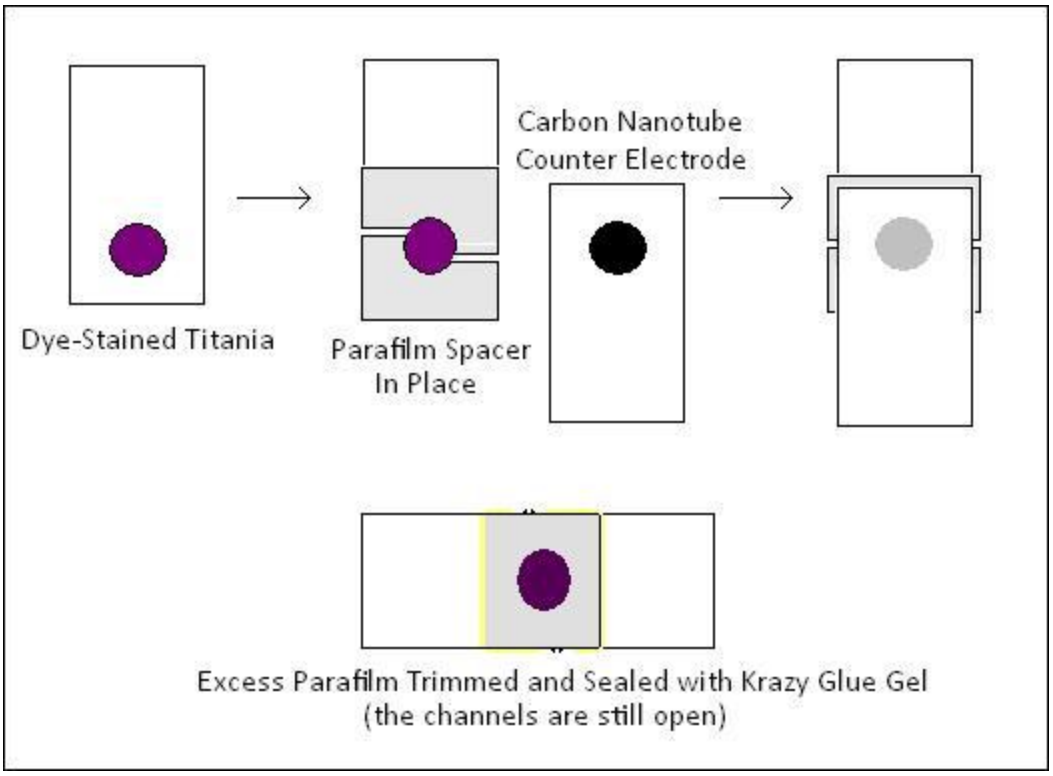

Figure 9. Dye-Sensitized Solar Cell Assembly

Preparation of the Electrolyte in Organic Solvent

In this project, "standard" dye-sensitized solar cells were fabricated using acetonitrile as the electrolytic organic solvent. These cells were used as a baseline comparison against the dye-sensitized solar cells using ionic liquids and polymer electrolytes that were the focus of this study.

The organic solvent electrolyte solution was made with lithium iodide (LiI), solid iodine (I_2), 4-*tert*-butylpyridine (BuPy), and acetonitrile. Specifically, 1.3485 g LiI was dissolved in 10.00 mL of acetonitrile. A second 10.00 mL flask was used to dissolve 0.2537 g of I_2 in acetonitrile. These solutions were mixed together in an amber bottle and 1.0 mL of 4-*tert*-butylpyridine was added. These amounts were determined based upon the final desired concentrations to be 0.50

M iodide, 0.05 M iodine, and 0.3 M BuPy. These concentrations are accepted as the optimized electrolyte concentrations and are routinely reported in dye-sensitized solar cell research.

Final Sealing Procedure

Injection of the electrolyte into the fabricated dye-sensitized solar cell occurred due to the capillary forces of the narrow channels left in the cell spacer. A very small drop of electrolyte was sufficient to fill the entire vacancy of the cell, but it was necessary to ensure that the vacancy was completely filled. Full channels indicate sufficient electrolyte has been added.

Using a pipette or eye dropper, a small drop of electrolyte, mass approximately 0.025 g, was placed at the channel opening. The electrolyte was observed to be pulled in and through the cell vacancy. Refer to Figure 10, below, for illustration of this capillary effect. If more electrolyte solution was needed to fill the void, another very small drop was used.

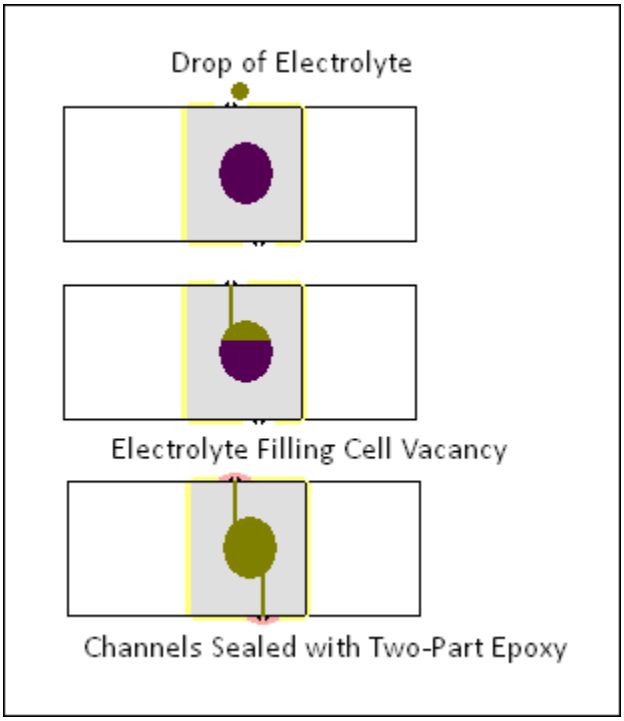

Figure 10. Electrolyte Injection and Cell Sealing

Once the cell was filled with electrolyte in acetonitrile solvent, the cell was tested in the solar simulation to ensure device functioning. The cell was then refilled with electrolyte and the channel openings were sealed using 3M two part epoxy. The epoxy was mixed and allowed to thicken for a minute before being applied to the channel opening. Once the epoxy dried, the cell was tested.

Application of Ionic Liquid Electrolyte and Device Sealing

The ionic liquids were too viscous to be drawn into the cell via the side channels. Instead, one drop was applied to the surface of the dyed titania and the counter electrode was firmly pressed down, making sure to minimize electrolyte seepage onto the Parafilm®. Since the weight percentage of ionic liquid relative to the polymer membrane was a studied variable, the ionic liquid application was done on the analytical balance. Once the device was shown to function under illumination, device sealing proceeded using the two-part epoxy.

Synthesis of poly(diallyldimethylammonium iodide), poly(DADMAI), Thin Films

The polymer poly(diallyldimethylammonium chloride), poly(DADMAC), is a cheap, readily available, non-toxic, flocculating agent used in wastewater treatment [81]. It has also been studied as a hydrogel for biomedical applications and as a component of highly ordered nanoparticulate polymer composites [82, 83, 84]. It dissolves into a cationic polymer backbone and counter chloride ions when placed in water. Poly(DADMAC) comes in a variety of molecular weights (from <100,000 g/mol average to 400,000 – 500,000 g/mol average for this study), and can be purchased in as high as 60 weight percent polymer solution in water.

A simple one step ion exchange was used to precipitate poly(diallyldimethylammonium iodide), poly(DADMAI), from aqueous poly(DADMAC). A visual confirmation of the reaction was

performed by observing a clear and colorless solution of potassium iodide, KI, mixed into a clear and colorless aqueous stock solution of poly(DADMAC). This mixing resulted in the immediate formation of a yellow-white gelatinous precipitate, which was thought to be poly(DADMAI) due to the high solubility of potassium chloride, KCl, in water.

$$K^+_{(aq)} + I^-_{(aq)} + pDADMA^+_{(aq)} + Cl^-_{(aq)} \rightarrow K^+_{(aq)} + Cl^-_{(aq)} + pDADMAI_{(s)}$$

The solid yellow-white precipitate was collected via centrifugation. The solid was collected and dried on a hotplate at 50 °C until observed to be free of moisture. The fact that no peak was observed at or around 100 °C during differential scanning calorimetry (DSC) confirmed no residual water was left in the polymer. The elemental composition was confirmed using electron dispersion spectroscopy (EDS) in conjunction with the scanning electron microscope (SEM). However, it was realized that formation of poly(DADMAI) films would be difficult, as it did not exhibit a melt temperature, nor did it go into a variety of typical polymer solvents (including water, acetone, methanol, ethanol, acetonitrile, dichlorobenzene, and DMSO).

Development of Electrolytic Polymer Membranes Swelled with Ionic Liquid

Thin films of poly(DADMAC) were made by dropcasting a 10 weight percent polymer solution over a two piece thick Scotch® tape template on a glass plate. This glass plate was then placed on a hotplate at 50 °C for about ten minutes. Water was driven off and the thin circular polymer membranes were recovered. If the films were heated for too long, they were observed to crack, and new films were made. These membranes were used in the poly(DADMAC) cell trials after saturation with predetermined quantities of ionic liquid. Additionally, poly(DADMAC) membranes made in the same manner were used to fabricate poly(DADMAI) membranes. This was accomplished by immersing the poly(DADMAC) membranes in a 2 M solution of potassium iodide in water. The polymer chloride ions slowly dissociated and iodide ions immediately

associated with the positively charged polymer backbone, keeping the polymer from going into solution completely. This process was thought to be diffusion limited and allowed to react for two days. After forty eight hours, the clear white polymer was observed to turn opaque and yellow. Films were removed, rinsed with distilled water to remove residual KI, and the elemental composition was again measured with SEM and EDS technologies. Complete conversion was observed.

The polymer films were then used in the previously discussed solar cell fabrication procedure for dye-sensitize solar cell production. The polymer membranes were weighed, saturated with ionic liquid, and weighed again to determine weight percent ionic liquid. The cell substrates were pressed together with the polymer membrane and ionic liquid sealed between. Cell testing was performed after thirty minutes had elapsed. Once the cell has been deemed to function, the cell sealing procedure commenced using the two-part epoxy.

Direct Drop Casting of Polymer Membranes onto Counter Electrodes

Polymer films fabricated in the previously discussed method were very brittle, fragile, and difficult to work with. It was of great interest to develop a method of depositing poly(DADMAC) and poly(DADMAI) films directly onto the cell substrate without interfering with the internal functionality of the solar cell. Ultimately, this is beneficial from a processing point of view and would greatly increase the feasibility of scale up processes. Additionally, in lab scale trials, it was difficult to develop identical films and identical ionic liquid mass ratios between cells. The poly(DADMAC) films were very flimsy and weak, while the poly(DADMAI) films were extremely brittle and delicate. Both were subject to warping after dehydration, and the breaking of these films was almost a guaranteed occurrence. A method of direct deposition was developed to avoid the issue of forming, transferring, sealing, and the inherent breaking of the

thin films inside the cell device. However, this method was not developed until after the full set of experiments had been performed.

These final solar cells contained poly(DADMAC) films which were directly cast from a 10 wt% poly(DADMAC) solution. This solution was directly deposited onto the carbon nanotube substrate and dehydrated on the hotplate. Results revealed poly(DADMAC) cells to achieve only an average of 0.20% power conversion efficiency. However, a set of poly(DADMAC) direct deposit cells were placed into the 2 M potassium iodide solution for 48 hours to successfully generate poly(DADMAI) films on the carbon nanotube surface. These cells reported an average power conversion efficiency of over 1.00%. This shows that not only does the direct deposition study have merit as future work, the poly(DADMAI) films are superior to the poly(DADMAC) films and may yet hold a meaningful purpose in dye-sensitized solar cell research.

Current-Voltage Characterization

Current-voltage characterization was performed by running a voltage sweep across the solar cell and measuring the electrical current output. The xenon lamp was calibrated to match actual solar power, AM 1.5 global conditions, using a pyranometer. The pyranometer measured this intensity by relating internal temperature change to the intensity of light output by the simulator. A light filter in the LS1000 Solar Simulator was used to match spectral output, but the light intensity was controlled by the input power to the bulb using the XPS1000 power source. AM 1.5 global output intensity of (1000 ± 10) W/m^2, or ± <1% accuracy was achieved.

AM 1.5 testing conditions dictate a reference temperature of 25 °C in addition to the spectral output. Since testing conditions were subject to increasing temperature, the method of testing was not consistent with AM 1.5 protocol and cannot be reported as such. The cells are being tested at appropriate spectral radiation under a standard light intensity of 1000 W/m^2.

The negative (black) terminal clip was connected to the top slide and the positive (red) terminal clip connected to the counter electrode slide. The cell was centered two inches below the glass dome of the simulator. The LabTracer 2.0 software program was opened and the Keithley source meter turned on. Voltage sweeps were conducted and data was collected.

The data text file was copied into an Excel spreadsheet to calculate the open circuit voltage (V_{oc}), short circuit current density (J_{sc}), voltage max (V_{max}), current density max (J_{max}), fill factor (FF), and power conversion efficiency (PCE). See Appendices A and B for more information regarding these characteristics.

Plots of the current density vs. voltage, as well as the power output vs. voltage, were also generated. The maximum point on the power output curve corresponds with the J_{max}, V_{max} point of the current density-voltage curve. This is because J_{max} and V_{max} correspond to the point on the current-voltage curve where power output is maximized, not the maximum current density or the maximum voltage.

CHAPTER VI

INTERPRETATION OF DATA

Standard Dye-Sensitized Solar Cell Data

Dye-sensitized solar cells using acetonitrile electrolyte solvent were created as standard solar cells for baseline comparison to the solar cells developed using ionic liquids and polymer membrane electrolytes. Current-voltage data was collected for standard cells under both illuminated and dark environments. From the results of these ten cells, an average short circuit current density of 7.8 mA/cm^2 , open circuit voltage of 0.65 V, and fill factor of 47% were determined, resulting in an average power conversion efficiency of 2.34%. These averages are summarized below in Table 5, along with high and low values for each parameter. Standard cells are identified as standards by the notation ST, followed by the batch number, individual cell letter, and either L or D (denoting light characterization or dark characterization), such as cell ST2AL seen in Figure 11.

Table 5. Parameter Averages for Standard Dye-Sensitized Solar Cells using Acetonitrile Electrolyte Solvent

Parameter	<Average>	High	Low
J_{sc} / (mA /cm^2)	7.78	9.62	5.87
V_{oc} / (V)	0.652	0.679	0.598
J_{max} / (mA/cm^2)	6.11	7.26	5.02
V_{max} / (V)	0.384	0.406	0.345
FF / %	47	55	40
PCE / (%)	2.34	2.88	1.98

Current-voltage data and dark current sweeps of the standard DSSC using acetonitrile solvent are shown in Figures 11 and 12, respectively. As shown in Figure 11, the open circuit voltage is quite reproducible, while the current density shows more variation. This makes sense, since voltage is determined by material properties and structural arrangement, while current density is subject to device fabrication and sealing (which is subject to much more technician error). However, the slopes of the data exhibit good reproducibility. This shows the shunt and series resistance in each cell behaves similarly, which indicates the cells have been developed in a consistent manner. Shunt resistance is a desired internal resistance; it functions as "walls" which direct current along a desired pathway, while the series resistance is desired to be low, so that current can flow readily in one direction. Calculation of these values was not an objective of this project, but a long flat portion of the current-voltage curve (slope = 0) indicates a high shunt resistance, while low series resistance is depicted by the vertical nature (slope = ∞).

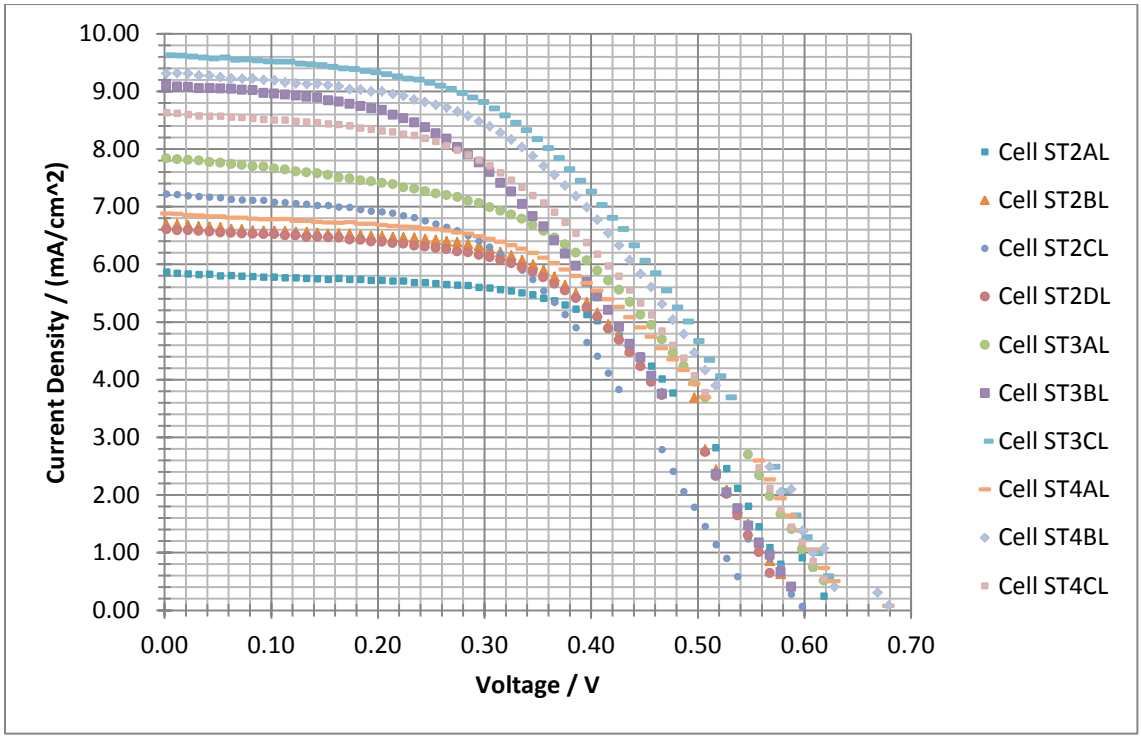

Figure 11. Illuminated Characterization of Dye-Sensitized Solar Cells at 1000 W/m^2 using Acetonitrile Electrolyte Solvent

Dark current characterization is necessary to determine if any current is being produced when the cell is not illuminated. The additive 4-tertbutylpyridine combats this effect, and Figure 12 shows that there is no observable current in the cells until a threshold voltage of 0.48 V is reached. At this point, enough potential is being applied to force current to flow through the cell even though it is not illuminated. Of all cells tested, all dark currents were observed to be negligible, so no further dark current graphs will be mentioned in this report.

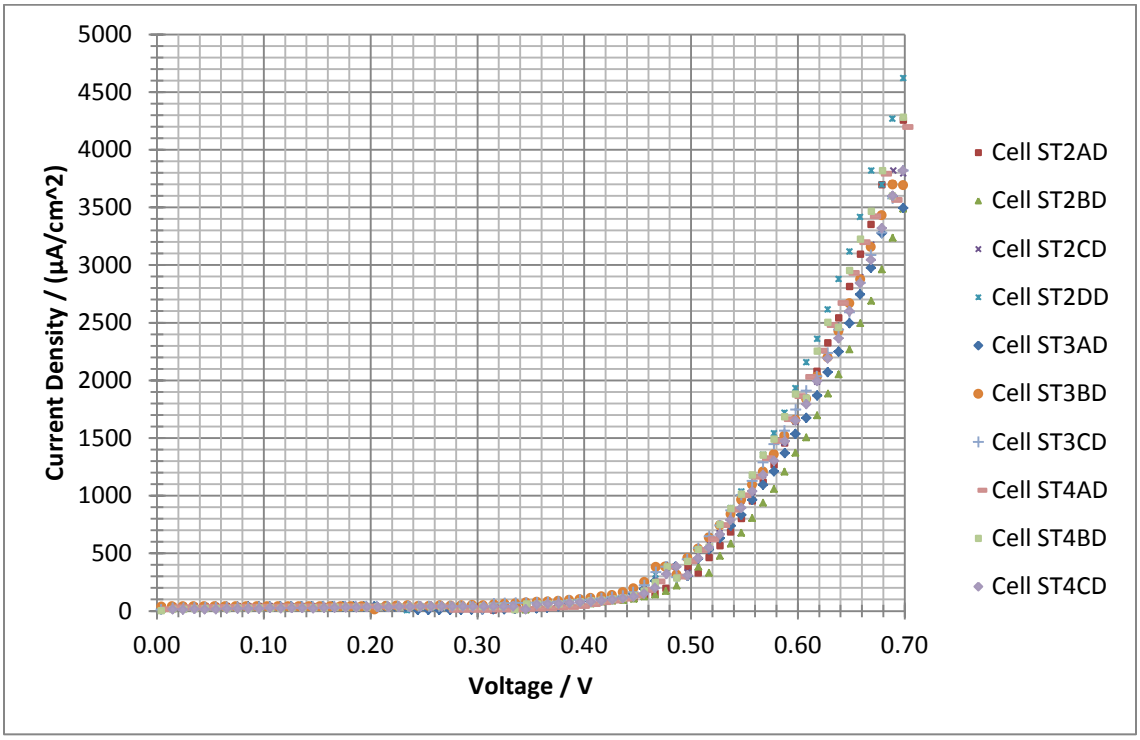

Figure 12. Dark Characterization of Dye-Sensitized Solar Cells using Acetonitrile Electrolyte Solvent

Additionally, dye-sensitized solar cells were produced using pure ionic liquid as solvent for comparison to both the standard acetonitrile based solvent solar cells and the composite ionic liquid – polyelectrolyte membrane solar cells. The results of these four cells are shown in Table 6 and in the illuminated current-voltage graph Figure 13, both shown on the next page.

Table 6. Parameter Averages for Solar Cells using Pure Ionic Liquid as Electrolyte Solvent

Parameter	<Average>	High	Low
J_{sc} / (mA /cm^2)	9.26	10.04	8.82
V_{oc} / (V)	0.452	0.477	0.416
J_{max} / (mA/cm^2)	5.30	6.18	4.78
V_{max} / (V)	0.237	0.255	0.214
FF / %	30	35	28
PCE / (%)	1.25	1.45	1.15

An average power conversion efficiency of 1.25% was achieved, but it is apparent in Figure 13 that a poor fill factor was achieved in these cells. The current-voltage trend appears almost linear, indicating a very poor shunt resistance (which therefore allows current to drain throughout the cell). Future trials may require better fabrication techniques, and longer times to allow sufficient electrolyte penetration into the titania structure.

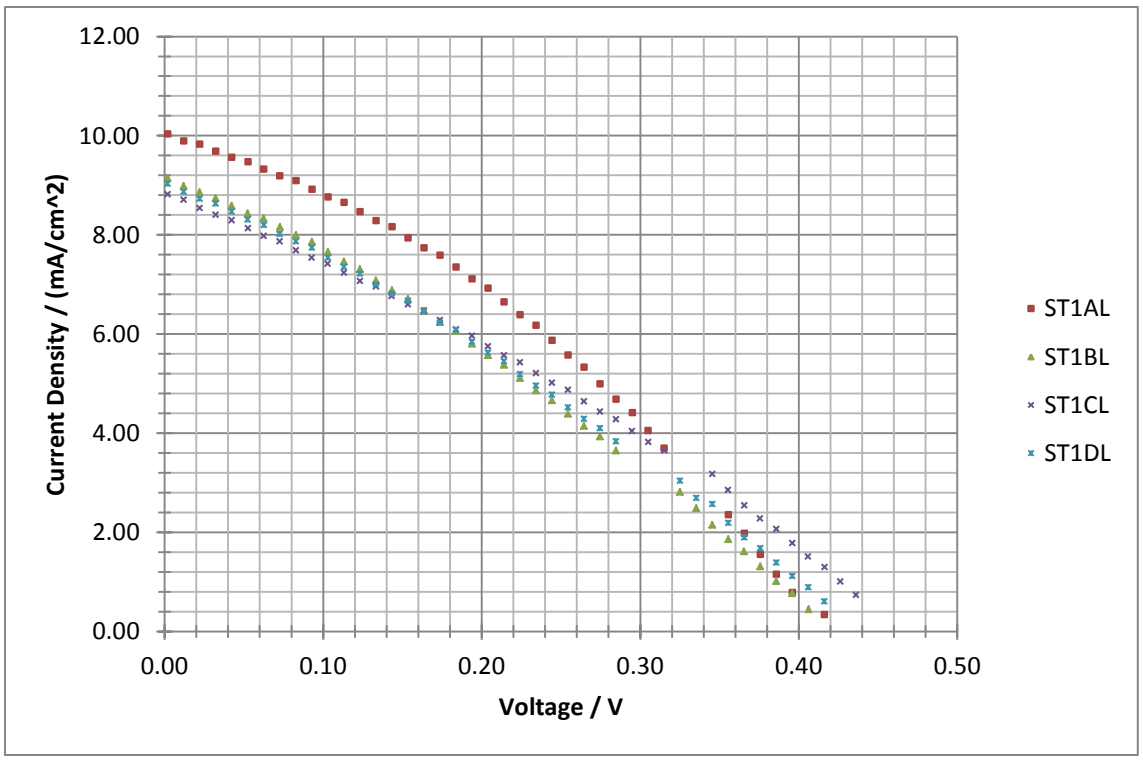

Figure 13. Illuminated Characterization of Dye-Sensitized Solar Cells at 1000 W/m^2 using Pure Ionic Liquid as Electrolyte Solvent

A comparison of these cells to other findings shows that both the acetonitrile solvent cells and the ionic liquid cells performed much lower than other reports. Of primary note is the difference in fill factors, which are often reported in the range of 60%. Since the cells reported in this study achieve only 30% fill factor, they are achieving only half the performance output as the cells in other references. Additionally, most standard cells are tested using a platinum counter electrode which was unavailable for this study. However, other carbon nanotube applications are achieving results only slightly higher than the standard acetonitrile solvent cells of this report [70, 75]. The carbon nanotube counter electrode is certainly a subject for future work.

Quantification of poly(DADMAC) and poly(DADMAI) Thin Films

Once standard cells were fabricated and tested, the ion exchange procedure was quantified. Stock solution poly(DADMAC) was used to produce thin film membranes which were then subjected to elemental analysis by Energy Dispersion Spectroscopy (EDS) in conjunction with a Scanning Electron Microscope (SEM). Images were recorded and surface analysis was conducted at 35x, 300x, and 1000x magnification for both poly(DADMAC) and poly(DADMAI) samples. These results were compared to theoretical elemental composition calculations.

The structure of both poly(DADMAC) and poly(DADMAI) is shown in Figure 14. The elemental composition of poly(DADMAC) by weight is 59.4 wt% carbon, 10.0 wt% hydrogen, 21.9 wt% chloride, and 8.7 wt% nitrogen. Substituting an iodide for chloride, the theoretical composition by weight of poly(DADMAI) is 38.0 wt% carbon, 6.4 wt% hydrogen, 50.1 wt% iodide, and 5.6 wt% nitrogen.

As shown in Table 7, the expected composition of poly(DADMAC) was accurately determined by EDS within the limitations of the instrument. Elements of very low molecular weight, such as hydrogen, helium, and lithium, are undetectable by EDS. Therefore, the weight

percent associated with hydrogen will be detected as another elemental mass. Also, because nitrogen is in a quaternary bound state, the change in energy associated with nitrogen excitation (due to electron beams bombarding its surface) will not be detected by the EDS apparatus.

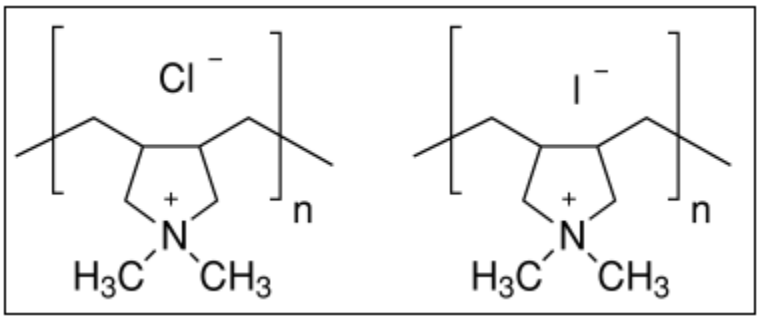

Figure 14. Repeat Unit of poly(DADMAC) and poly(DADMAI)

Therefore, the weight percent associated with nitrogen will also be detected as another mass percentage. However, in this study, the primary concern falls on the expected weight percent of chloride and iodide in poly(DADMAC) (which are expected to be 21.9% and 0.0%, respectively) and the expected weight percent of chloride and iodide in poly(DADMAI) (which are expected to be <1.0% and 50.1%, respectively). These anticipated numbers were confirmed by the results of the EDS trials, shown in Tables 7 and 8. Potassium was also analyzed due to the fact that it may crystallize as potassium iodide on the surface of the poly(DADMAI) films if the films are not thoroughly rinsed in de-ionized water. An image of this undesired crystallization is shown in Figure 15 (next page). As expected, poly(DADMAC) films contain a range of 16 to 32 wt% chloride (where 22 wt% was expected). Since no ion exchange has been conducted, both the potassium and iodide content were determined to be statistically 0.0 wt%, which are the expected values for poly(DADMAC).

Table 7. Elemental Composition of poly(DADMAC) films

35x		300x		1000x	
Element	wt %	Element	wt %	Element	wt %
MW <100,000 g/mol					
C	77.8 ± 2.9	C	78.6 ± 3.1	C	77.9 ± 3.1
N	0.0 ± 0.0	N	0.0 ± 0.0	N	0.0 ± 0.0
Cl	21.9 ± 5.9	Cl	21.1 ± 6.0	Cl	21.7 ± 6.2
I	0.2 ± 0.3	I	0.2 ± 0.1	I	0.2 ± 0.3
K	0.04 ± 0.2	K	0.05 ± 0.2	K	0.08 ± 0.3
MW 400,000 – 500,000 g/mol					
C	73.4 ± 2.2	C	74.1 ± 2.4	C	74.7 ± 2.5
N	0.0 ± 0.0	N	0.0 ± 0.0	N	0.0 ± 0.0
Cl	26.3 ± 5.7	Cl	25.5 ± 5.7	Cl	25.0 ± 5.9
I	0.2 ± 0.2	I	0.3 ± 0.3	I	0.2 ± 0.2
K	0.02 ± 0.1	K	0.03 ± 0.2	K	0.06 ± 0.2

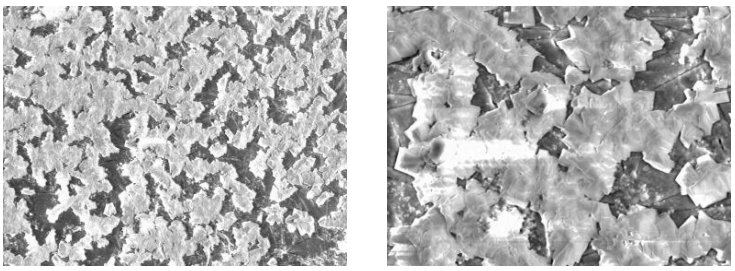

Figure 15. Examples of poly(DADMAI) film Covered in Potassium Iodide Crystal

The composition of poly(DADMAI) was shown to be within reasonable values of the theoretical calculations. As shown in Table 8, both chloride and potassium values were determined to be statistically 0.0 wt%, indicating complete removal of both chloride and potassium ions was achieved. This was the desired goal. However, iodide wt% was determined to range from 42.9 to 49.9 wt%, which is slightly lower than the 50.1% expected theoretical value. Since EDS confirmed complete chloride removal, it is surmised that the wt% of nitrogen and hydrogen are being attributed to carbon mass and lowering the EDS calculated iodide composition.

Table 8. Elemental Composition of poly(DADMAI) films

35x		300x		1000x	
Element	wt %	Element	wt %	Element	wt %
MW <100,000 g/mol					
C	53.3 ± 2.6	C	55.8 ± 2.8	C	56.0 ± 2.9
N	0.0 ± 0.0	N	0.0 ± 0.0	N	0.0 ± 0.0
Cl	0.2 ± 0.4	Cl	0.2 ± 0.4	Cl	0.2 ± 0.4
I	45.9 ± 3.0	I	43.6 ± 3.1	I	43.2 ± 3.1
K	0.6 ± 0.6	K	0.4 ± 0.6	K	0.6 ± 0.7
MW 400,000 – 500,000 g/mol					
C	52.4 ± 2.4	C	53.2 ± 2.5	C	55.3 ± 2.7
N	0.0 ± 0.0	N	0.0 ± 0.0	N	0.0 ± 0.0
Cl	0.1 ± 0.6	Cl	0.2 ± 0.3	Cl	0.1 ± 0.2
I	47.1 ± 2.8	I	45.9 ± 2.9	I	44.2 ± 3.0
K	0.4 ± 0.5	K	0.7 ± 0.7	K	0.4 ± 0.6

For each magnification of poly(DADMAC) and poly(DADMAI) samples in Tables 7 and 8, an SEM image was recorded for viewing surface characteristics. The poly(DADMAC) images are summarized in Figures 16 and 17, and poly(DADMAI) images in Figures 18 and 19.

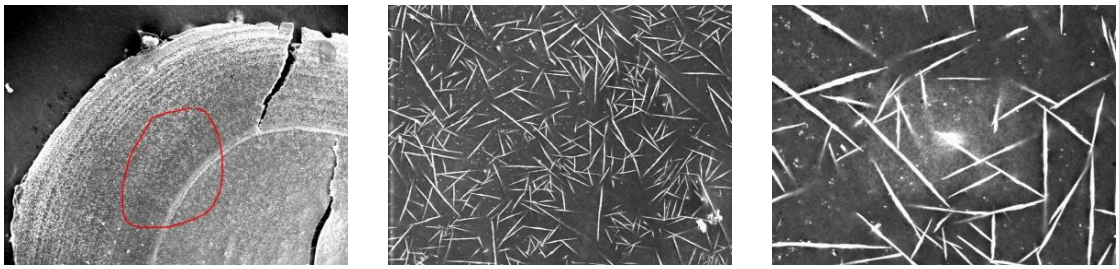

Figure 16. Surface Characteristics of <100,000 g/mol poly(DADMAC) at 35x, 300x, 1000x

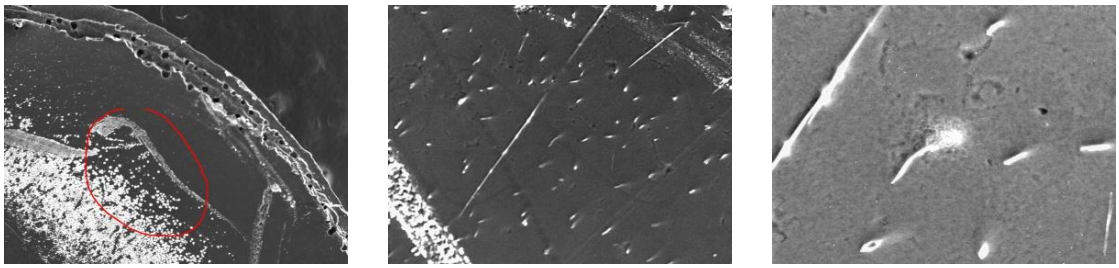

Figure 17. Surface Characteristics of 400,000 - 500,000 g/mol poly(DADMAC) at 35x, 300x, 1000x

The poly(DADMAC) surface is completely solid and there are no holes or void spaces apparent at this level of magnification. The jagged lines in Figure 16 are thought to be supramolecular ordered structures which form as the water is evaporated from a poly(DADMAC) solution. When dissolved, the polymer assumes an energetically favorable elongated conformation. This conformation is maintained to a small degree when the polymer is dried, but no bulk crystallinity can be assigned to this polymer phase. It is thought this conformation may be energetically unfavorable, but due to the slow rate of water evaporation, this structure was achieved. These linear structures are observed in both high and low molecular weights, although the <100,000 g/mol poly(DADMAC) appears to achieve a higher degree of ordering.

The poly(DADMAI) images appear to display the reverse trend. Both poly(DADMAI) film weights were developed from corresponding poly(DADMAC) films. Therefore, the surface characteristics would be expected to transfer from one polymer type to the other. However, in Figure 18, low molecular weight poly(DADMAI) seems to exhibit no structural ordering like those seen in Figures 16 and 17.

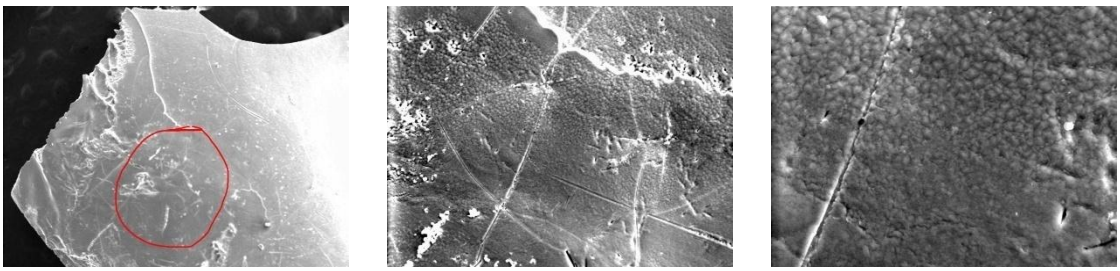

Figure 18. Surface Characteristics of <100,000 g/mol poly(DADMAI) at 35x, 300x, 1000x

There are some void spaces, and possibly a stress fracture in the film. The actual surface looks to be rough, especially compared to the flat and smooth poly(DADMAC) surfaces. In contrast, the high molecular weight poly(DADMAI) in Figure 19 displays jagged depressions which could be a result of the assembled polymer microstructure phases. The surface also

appears rather smooth compared to the <100,000 g/mol poly(DADMAI), despite the jagged voids in the polymer sample.

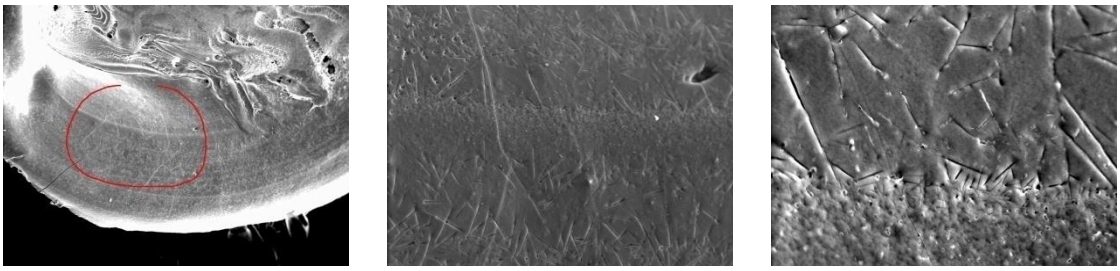

Figure 19. Surface Characteristics of 400,000 - 500,000 g/mol poly(DADMAI) at 35x, 300x, 1000x

Verification of Polymer Synthesis by Thermal Scanning

Differential scanning calorimetry was employed to determine if the ion exchange resulted in a change in the polymer glass transition temperature. Upon heating during the DSC trials, no glass transition temperatures or melt temperatures were observed for poly(DADMAI). However, a large peak did appear on first scans only (and not on replicate scans of the same sample) as shown in Figure 20. The cause of this peak is not known for certain, but it may be attributed to polymer relaxation as the microstructured phase is released from its "trapped" configuration. This trapping is caused by electrostatic interactions of the polymer backbone while it slowly comes out of solution [85, 86.] This mystery DSC peak is not gasification of the polymer (the sealed aluminum pans did not explode as in other failed DSC trials), and a polymer reaction (such as cross linking) seems unreasonable given the composition of poly(DADMAI) and extremely low amounts of residual initiator potentially contained in the stock polymer.

As discussed above, samples of poly(DADMAC) and poly(DADMAI) were subjected to differential scanning calorimetry to determine if changes in the glass transition temperature of the polymer occurred after the ion exchange was performed. The most noteworthy change was the poly(DADMAC) glass transition temperature was completely removed upon the ion

exchange reaction. In Figure 20, the glass transition temperature for poly(DADMAC) is noted at 68 °C, which agrees with previous reports [87]. This glass transition temperature reappears on every thermal scan for poly(DADMAC). The fact that no glass transition temperature was apparent for poly(DADMAI) confirms that the secondary polymer had been synthesized.

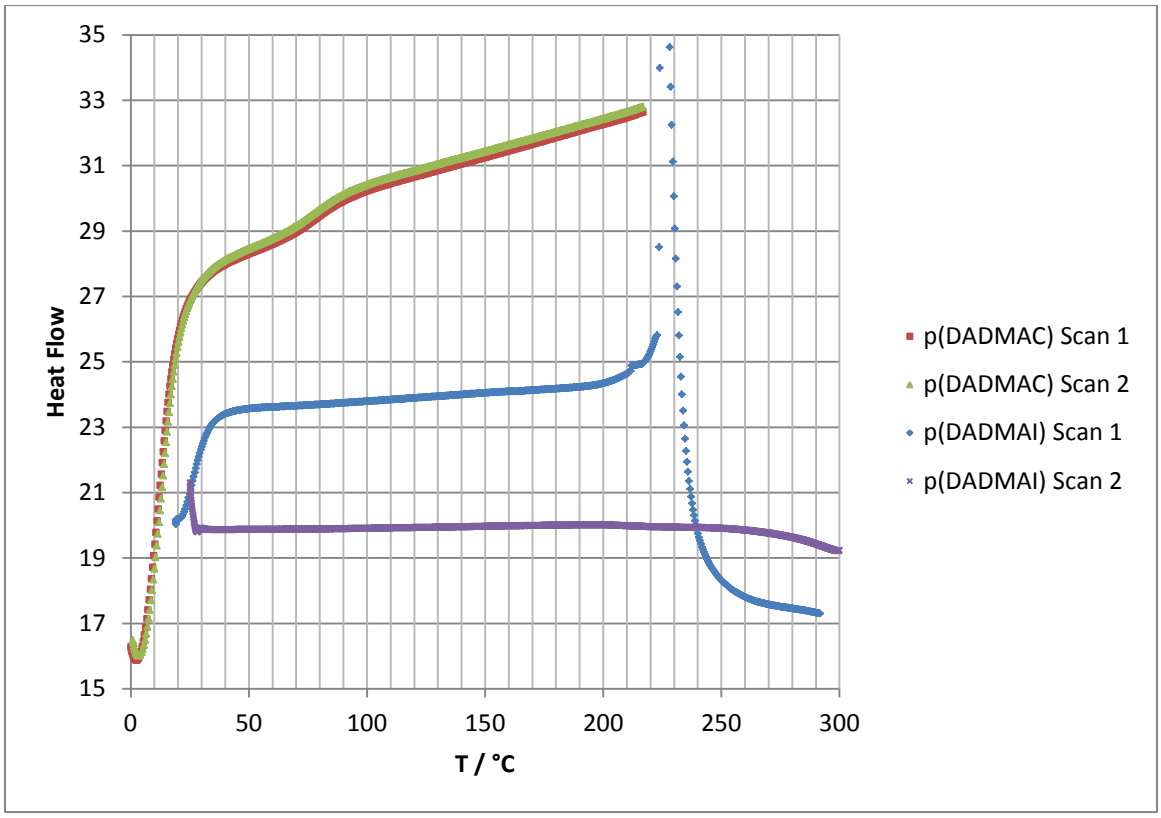

Figure 20. Determination of Glass Transition Temperature in poly(DADMAC) and poly(DADMAI)

poly(DADMAC) Membrane Electrolyte Data Analysis

Polyelectrolyte membranes were developed according to the experimental design for the poly(DADMAC) polymer as discussed in Tables 3 and 4. The mass of these membranes was an average of 0.0050 g. Four replicates were conducted to determine the significance of any effect or interaction of variables in the poly(DADMAC) films. Additionally, if variables were shown to be insignificant and appropriate rationale could be determined, a simplified experimental design could be developed for the second half of this study regarding the novel

polymer poly(DADMAI). Evaluation of the Power Conversion Efficiency (PCE) was conducted in Minitab to determine the significance of effects. The poly(DADMAC) data is tabulated in Table 9, shown below.

Table 9. Summary of poly(DADMAC) Electrolyte Parameter Evaluation

Cell Identification	PCE / %	J_{SC} / (mA/cm^2)	V_{OC} / V	FF / %
100H72C-A	0.62	4.632	0.527	25.4
100H65C-B	0.90	5.708	0.487	32.4
100H74C-C	0.57	4.212	0.538	25.0
100H67C-D	1.06	7.135	0.548	27.2
100H44C-A	0.89	5.802	0.527	29.2
100H59C-B	0.64	4.629	0.517	26.8
100H53C-C	0.57	5.909	0.487	19.8
100H53C-D	0.65	5.829	0.517	21.7
100B66C-A	1.10	6.556	0.467	35.8
100B68C-B	0.46	3.888	0.477	24.8
100B73C-C	1.00	5.817	0.467	37.0
100B71C-D	1.00	7.338	0.527	25.7
100B55C-A	0.98	6.786	0.507	28.4
100B55C-B	0.72	5.126	0.517	27.0
100B69C-C	0.31	2.358	0.547	24.3
100B55C-D	0.58	4.636	0.527	23.9
450H86C-A	0.65	4.433	0.588	24.9
450H73C-B	0.69	6.108	0.497	22.6
450H73C-C	0.24	1.887	0.538	23.2
450H65C-D	0.79	6.479	0.497	24.5
450H59C-A	0.99	5.242	0.527	35.8
450H62C-B	0.82	6.802	0.457	26.4
450H52C-C	0.36	3.824	0.457	20.7
450H52C-D	0.62	5.959	0.487	21.4
450B76C-A	0.33	2.979	0.477	23.4
450B73C-B	0.18	1.618	0.446	24.9
450B74C-C	0.38	4.584	0.416	19.7
450B72C-D	0.86	3.818	0.527	43.0
450B47C-A	0.22	1.915	0.467	24.9
450B55C-B	0.42	3.170	0.527	24.9
450B52C-C	0.59	5.055	0.487	24.1
450B52C-D	0.58	5.923	0.507	19.2
Average	0.65	4.880	0.503	26.2

The data in Table 9 is partitioned into each set of replicates (4 per partition). Cells are identified by molecular weight (100 relates to 100,000 g/mol, 450 relates to 400,000 – 500,000 g/mol), ionic liquid type (B for butyl imidazolium iodide, H for hexyl imidazolium iodide), weight percent ionic liquid as a two digit number (i.e. 73 denotes 73% ionic liquid by weight), polymer type (C for poly(DADMAC), I for poly(DADMAI)), and replicate (A, B, C, and D). Noteworthy cell parameters include a high fill factor of 43%, high open circuit voltage of 0.588 V, and high current density of 7.338 mA/cm^2. As previously mentioned, high fill factors directly relate to higher performing cells due to the simple fact that the power conversion efficiency calculation is scaled by the fill factor. Cells achieving exceptional current densities and voltages are therefore limited by poor fill factors. Open circuit voltage results showed the least variance between trials. This was expected since voltage is governed by material selection, which only varied in polymer molecular weight for this study. However, current density showed great variance, ranging from 1.618 to 7.338 mA/cm^2. This variance in current is attributed primarily to variance in the cell fabrication due to the difficulty in producing similar cells. Regardless, to achieve a high performance cell, both current density and fill factor must approach high end operation. For example, a cell with an average open circuit voltage of 0.503 V, high fill factor of 43.0, and short circuit high current density of 7.388 mA/cm^2 would have achieved a power conversion efficiency of 1.60%. This may seem low, but recall PEO solid state electrolytes only achieved 2.0% in other publications, and a 43.0 fill factor is still relatively low compared to other reports [54].

An average power conversion efficiency of 0.65% was achieved, but cells made with <100,000 g/mol poly(DADMAC) and hexyl imidazolium iodide were statistically superior. This performance corresponds with the suspected polymer microstructures observed in Figure 16, which may indicate a correlation between degree of microstructure ordering and cell performance.

The only statistically significant effect in the first half of this study was found to be the molecular weight of poly(DADMAC). The polymer to ionic liquid weight ratio effect was statistically insignificant over the range studied, as were all the interactions associated with this variable. This allowed it to be removed from the poly(DADMAI) experimental design setup. The alkyl chain length of the ionic liquid was retained due to a suspected interaction occurring between the ionic liquid and the polymer molecular weight. Figure 21 shows a Pareto chart of the poly(DADMAC) experiment variables and variable interactions. As can be seen, the only statistically significant t-score ($t > 2.064$) occurred for poly(DADMAC) molecular weight.

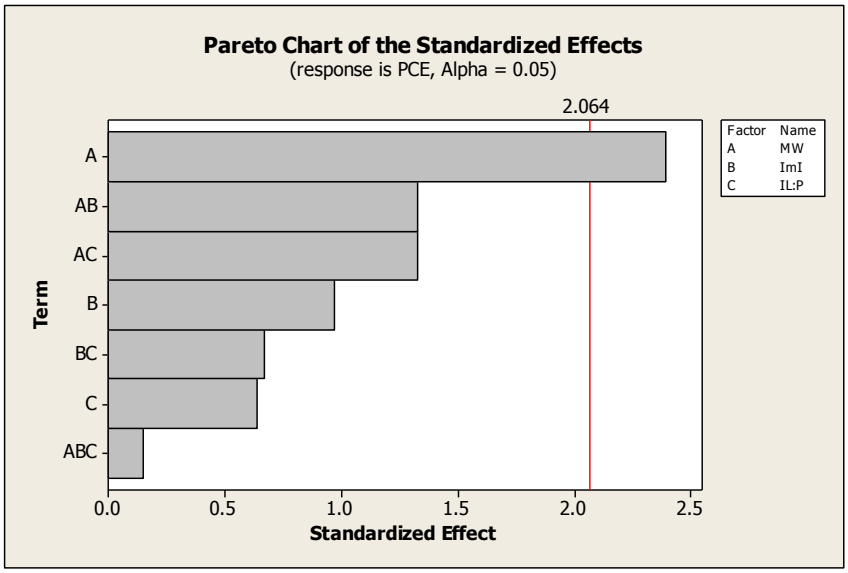

Figure 21. Pareto Chart Showing Significance of poly(DADMAC) Effects and Interactions

poly(DADMAI) Membrane Electrolyte Data Analysis

As discussed in Tables 3 and 4, the dye-sensitized solar cells made using poly(DADMAI) – ionic liquid electrolytes were performed in four replicates using variables of molecular weight and ionic liquid alkyl chain length. The results of these trials are found in Table 10. Cell identifications are of the same form as that of Table 9, while leaving out weight percent ionic liquid since it was not studied for poly(DADMAI) electrolytes (noted as "xx" in the table). The

most noteworthy parameter is the 56.9% fill factor achieved for cell 100HxxI-A. This fill factor is no doubt the cause of the 1.88% power conversion efficiency achieved by that particular solar cell. However, higher fill factors were consistently reported in poly(DADMAI) cells, even though the same fabrication procedure was used for both poly(DADMAI) and poly(DADMAC) cells. In fact, the average short circuit current density was higher for poly(DADMAI) by 25%, the average open circuit voltage was higher for poly(DADMAI) by 3%, and the average fill factor was higher for poly(DADMAI) by almost 24%. In particular, the highest performing cell electrolytes made of low molecular weight polymer and hexylimidazolium iodide ionic liquid achieved average power conversion efficiencies of 1.60% (compared to the highest performing poly(DADMAC) cells at 0.89%). This evidence suggests poly(DADMAI) membranes do facilitate some sort of additional transport mechanism resulting in higher fill factors, higher current densities, and higher voltages compared to those of poly(DADMAC).

Table 10. Summary of poly(DADMAI) Electrolyte Parameter Evaluation

Cell Identification	PCE / %	J_{sc} / (mA/cm^2)	V_{oc} / V	FF / %
100HxxI-A	1.88	5.014	0.659	56.9
100HxxI-B	1.38	6.281	0.619	35.6
100HxxI-C	1.82	5.688	0.679	47.1
100HxxI-D	1.33	6.350	0.588	35.5
100BxxI-A	1.09	8.802	0.487	25.5
100BxxI-B	1.60	8.950	0.538	33.2
100BxxI-C	1.26	7.915	0.528	30.2
100BxxI-D	0.67	6.159	0.426	25.6
450HxxI-A	0.78	5.908	0.497	26.6
450HxxI-B	0.75	5.949	0.477	26.3
450HxxI-C	1.01	5.441	0.517	35.8
450HxxI-D	0.16	2.146	0.356	21.5
450BxxI-A	1.18	6.480	0.507	36.0
450BxxI-B	0.75	6.199	0.437	27.7
450BxxI-C	0.29	3.338	0.447	19.4
450BxxI-D	1.29	6.983	0.528	35.0
Average	1.08	6.100	0.518	32.4

The Pareto chart in Figure 22 summarizes the significant interactions of the poly(DADMAI) study. Only the effects showing a t-score greater than 2.179 are significant, which in this case is only the polymer molecular weight. As was the case with poly(DADMAC), an interaction between ionic liquid and molecular weight seems to exist, but certainly ionic liquid alkyl chain length is not an important factor in this study. However, because the ionic liquid trials have been completely performed, the results will be included in the full factorial analysis of the data from both the poly(DADMAC) and poly(DADMAI) studies.

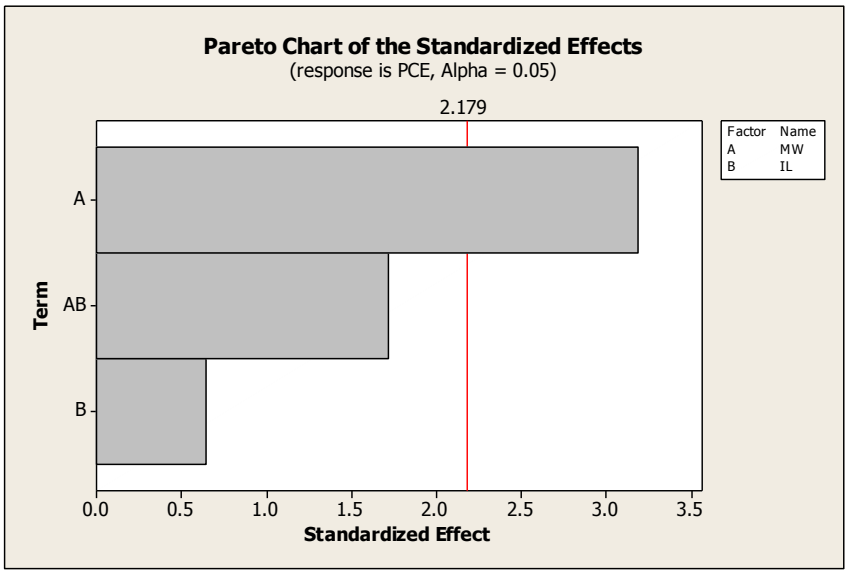

Figure 22. Pareto Chart Showing Significance of poly(DADMAI) Effects and Interactions

The combined data yielded a complete 2^3 full factorial design (as discussed in Tables 3 and 4). The Pareto chart, the cubic interactions summary, and contour plots for both poly(DADMAC) and poly(DADMAI) follow in Figure 23.

Fully Combined Experimental Analysis

The combined results Pareto chart, summarizing the entire experimental design, is shown in Figure 23. It was already determined the polymer molecular weight was statistically significant, and it should be apparent by the differences in high performing poly(DADMAC) and

poly(DADMAI) that the polymer type will prove to be of importance. This is indeed the case, as depicted in Figure 23. Other interactions noted from previous Pareto charts show no significance here. However, this is the first chart displaying the three-way interaction between the polymer type, polymer molecular weight, and ionic liquid alkyl chain length. Although this three-way interaction is still not significant, it is not so by only a small margin.

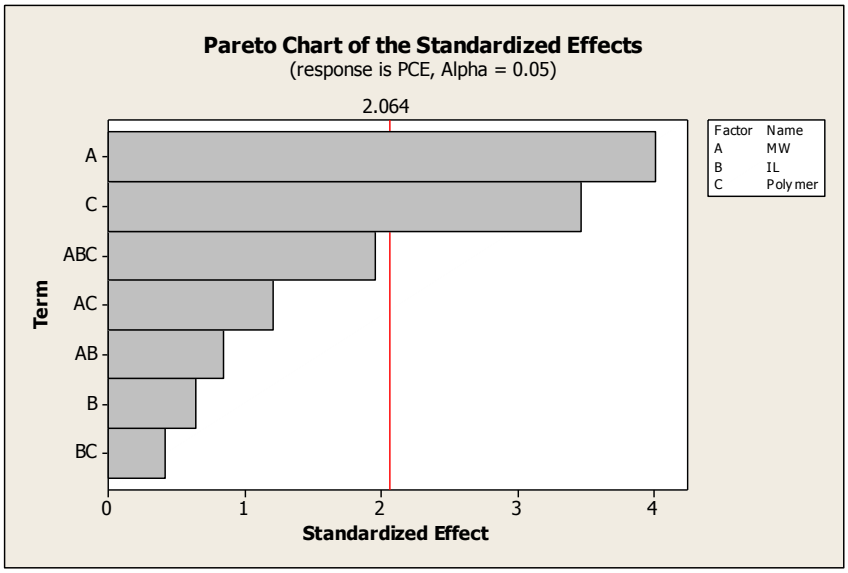

Figure 23. Combined poly(DADMAC) & poly(DADMAI) Pareto Chart Showing Significance of Effects and Interactions

The cubic interaction plot, on the next page in Figure 24, summarizes the 2^3 full factorial design by calculating the average power conversion efficiency for each set of 4 replicates tested at each set of conditions. The cubic dimensions correspond to polymer molecular weight (x-axis, where 1 corresponds to 100,000 g/mol and 4.5 corresponds to 400,000 – 500,000 g/mol), ionic liquid alkyl chain length (y-axis, where 4 corresponds to butyl and 6 corresponds to hexyl), and polymer type (z-axis, where Cl corresponds to poly(DADMAC) and I corresponds to poly(DADMAI)), This chart shows the averages compared earlier for highest performing poly(DADMAC) cells at 0.89%, highest performing poly(DADMAI) cells at 1.60%, and all other cell averages falling below these two values. It is apparent that both high performing polymer types

occurred when low molecular weight polymer was used. However, poly(DADMAC) electrolytes performed better with butyl imidazolium iodide, while poly(DADMAI) electrolytes performed better with hexyl imidazolium iodide. This result continues to fuel the thought that an interaction between polymer molecular weight and ionic liquid may be occurring, possibly due to steric and electronic interactions at the molecular level. It is also worth mentioning that the poorest performing poly(DADMAI) electrolyte still outperformed two of the poly(DADMAC) electrolytes. These results demonstrate the ability of poly(DADMAI) to achieve higher PCE than poly(DADMAC) in DSSC electrolytes.

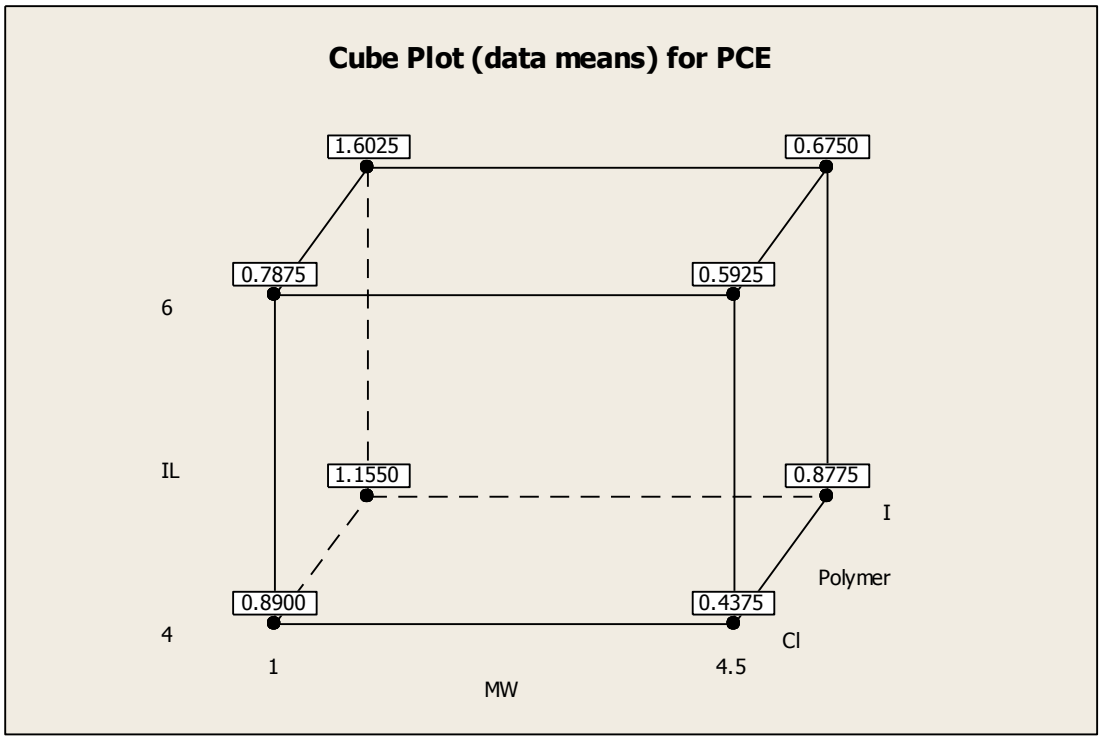

Figure 24. Cube Plot Summarizing Experimental Results

The contour plots for both poly(DADMAC) and poly(DADMAI) (Figures 25 and 26, respectively) show how optimization could be conducted if the three variables in this study could be scaled to reached full optimization. However, it is not feasible to perform such optimization tests because in this study, ionic liquid alkyl chain length ranges from butyl (4) to

hexyl (6), and polymer molecular weight ranges from 100,000 g/mol (denoted as 1 in the contour plot) to 400,000 – 500,000 g/mol (denoted as 4.5 in the contour plot). The polymer type composition could be optimized if varying degrees of ion exchange were performed, but this would require an experimental design containing center and star points. This was not a focus of the project, so high performing cells will be found to only occur at corner points in the design. Again, these contour plots simply echo the results of the cube plot in Figure 24, but they also show how the results statistically change as cell conditions deviate away from the high performance parameters. At the least, it should be concluded not to make poly(DADMAC) cells using high molecular weight polyelectrolyte and butyl imidazolium iodide because of the statistically poor performance of those cells. This poor performance is visualized by the light white area of Figure 25.

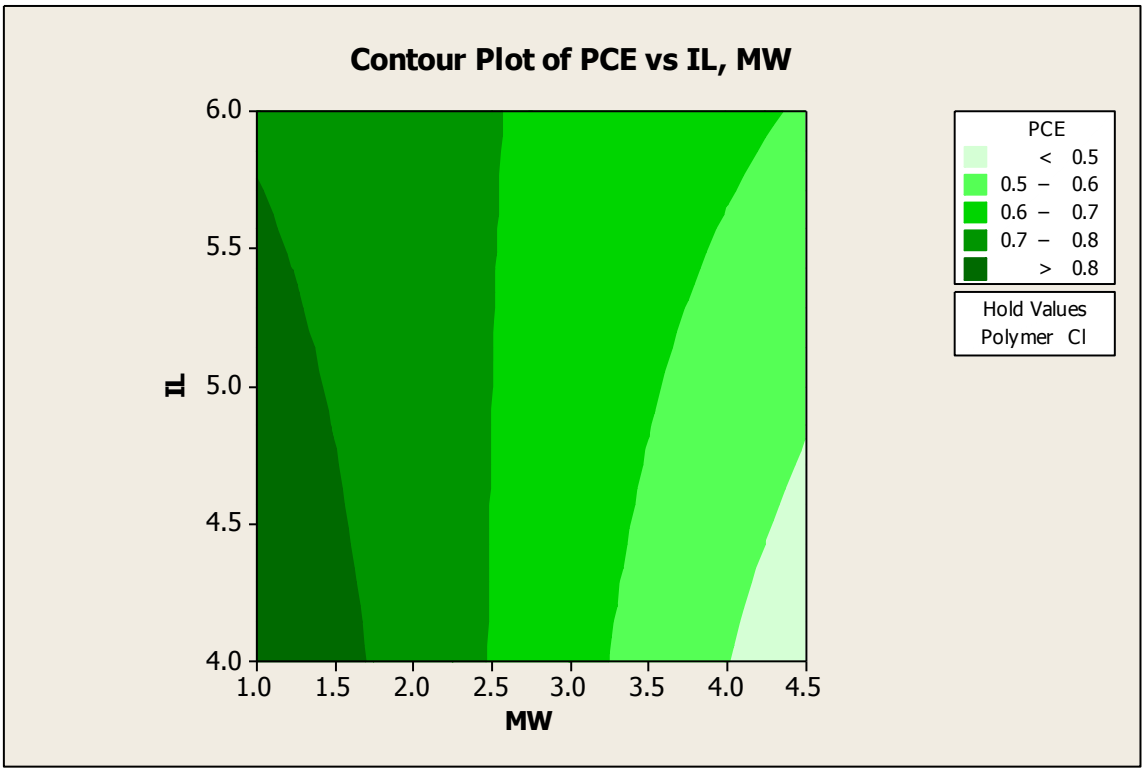

Figure 25. Contour Plot Showing Optimized poly(DADMAC) Solar Cell Variables

In contrast, the darkest area of Figure 26 corresponds to the high performance parameters of poly(DADMAI). Again, these parameters are shown to be a low molecular weight iodide polyelectrolyte in conjunction with hexyl imidazolium iodide ionic liquid. Illuminated current – voltage characterization curves are shown for these high performing poly(DADMAI) cells in Figure 27. Although some degree of variance in the current density is apparent in these four cells, the open circuit voltage remains centered around 0.64 V. This higher voltage is potentially due to the different electronic properties of the poly(DADMAI) electrolyte and a better performing solar cell was achieved.

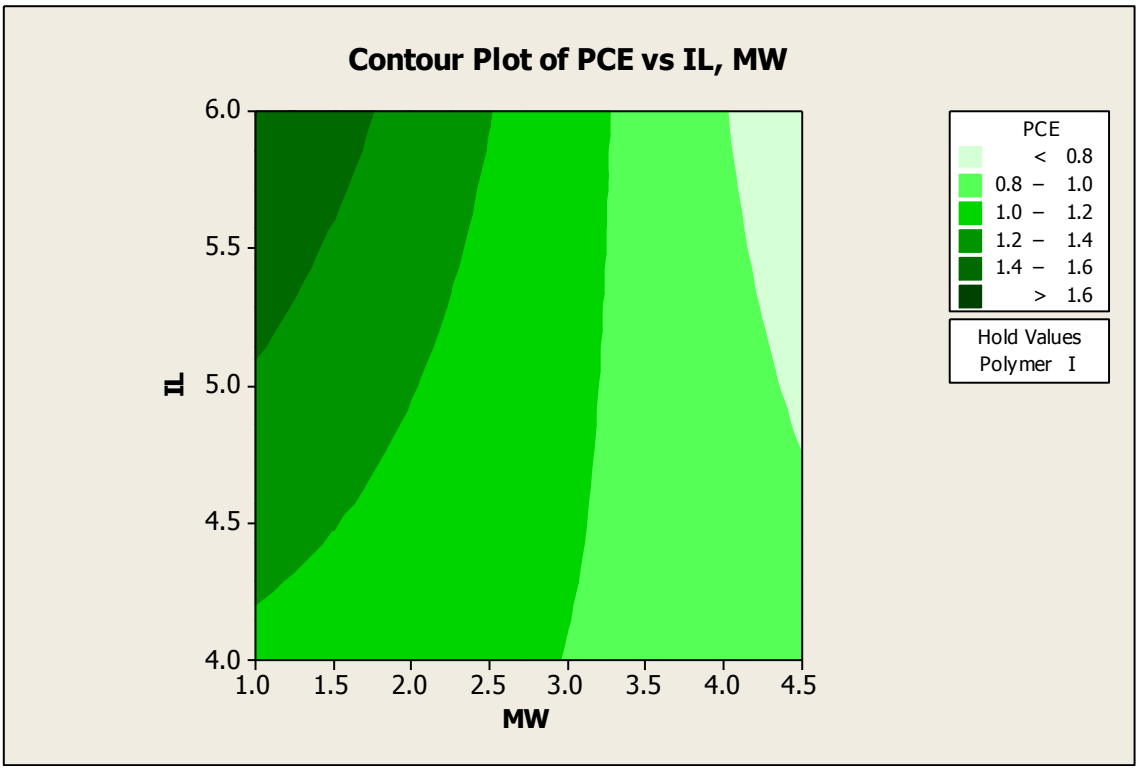

Figure 26. Contour Plot Showing Optimized poly(DADMAI) Solar Cell Variables

In Figure 28, the highest performing standard cell using acetonitrile electrolyte solvent is compared to the highest performing polymer-ionic liquid electrolyte solar cell. It becomes quite apparent where the limiting mechanism lies in producing high performance solid-state electrolytes. Although both cells followed similar fabrication procedures and relatively similar

electrolyte species (similar in the sense both used iodide as ionic transport), liquid redox electrolytes achieved almost twice the current density as that of the ionic liquid swelled polyelectrolytes developed in this study. Open circuit voltages only show an average of 3% increase with the novel poly(DADMAI) electrolyte compared to the acetonitrile organic liquid solvent, but this is not enough to offset the substantial decrease in ionic diffusion which resulted in poor current density. Future work is necessary to continue increasing current density, through both materials development and better cell fabrication methodology.

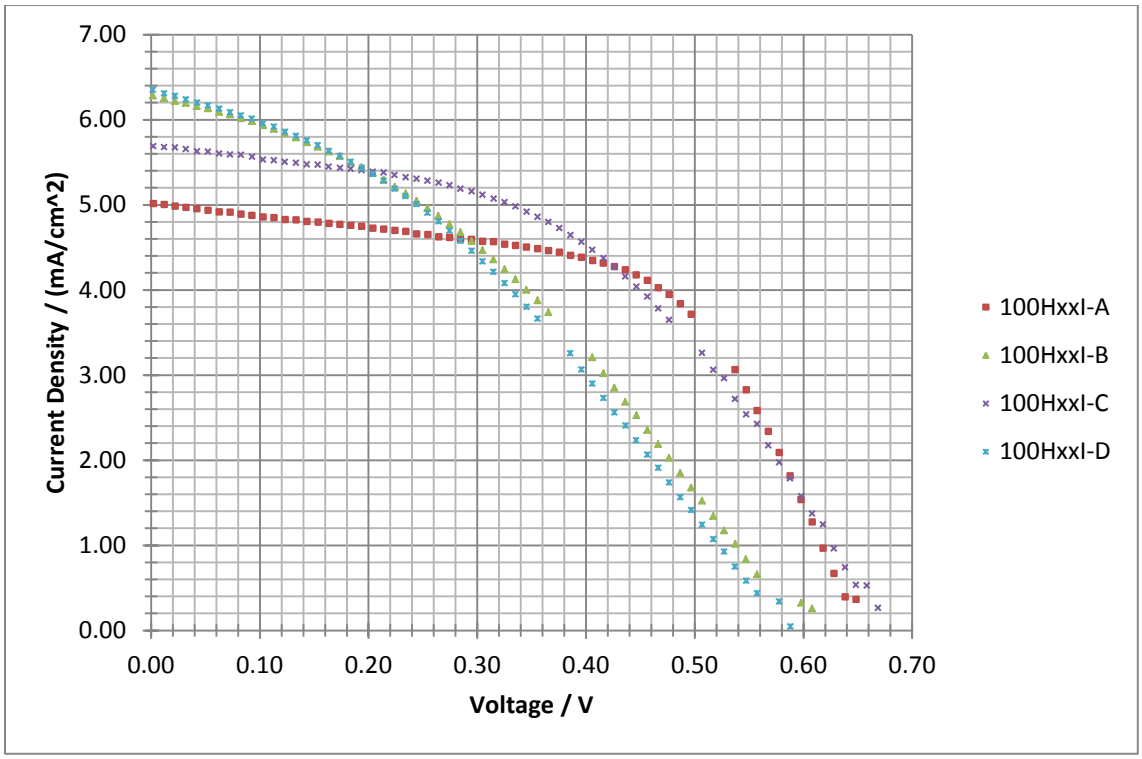

Figure 27. Current – Voltage Characterization of <100,000 g/mol poly(DADMAI) with Hexyl Imidazolium Iodide Electrolyte

Cell Performance after Forty-Five Days

Many studies do not report the longevity of laboratory cells because volatile organic liquids are used as the electrolyte solvent. These organic solvents evaporate quickly and are capable of permeating most glues and cell sealing pastes, making solar cell performance short

lived (on the order of magnitude of hours). For these devices to become practical, longevity must be achieved on the order of magnitude of years. If cell longevity tests are reported, the study is commonly performed at elevated temperatures for specified lengths of time. This may give insight into how electrolytes behave and how cells perform under extreme conditions, but it does not reveal lifetime data under normal operating conditions. To determine if the novel electrolyte material of this study would achieve higher cell stability and longevity, all swelled poly-electrolyte membrane solar cells were retested 45 days after initial testing. The power conversion efficiencies were again determined and the percent of power conversion efficiency retained was calculated.

During the 45 day wait, the cells were left sitting in normal atmospheric conditions on the laboratory bench top with the top electrode facing down. The cells were tested in the same manner as reported in their initial test date. The results are reported in Table 11 (next page) as a percentage of the initial power conversion efficiency retained after 45 days.

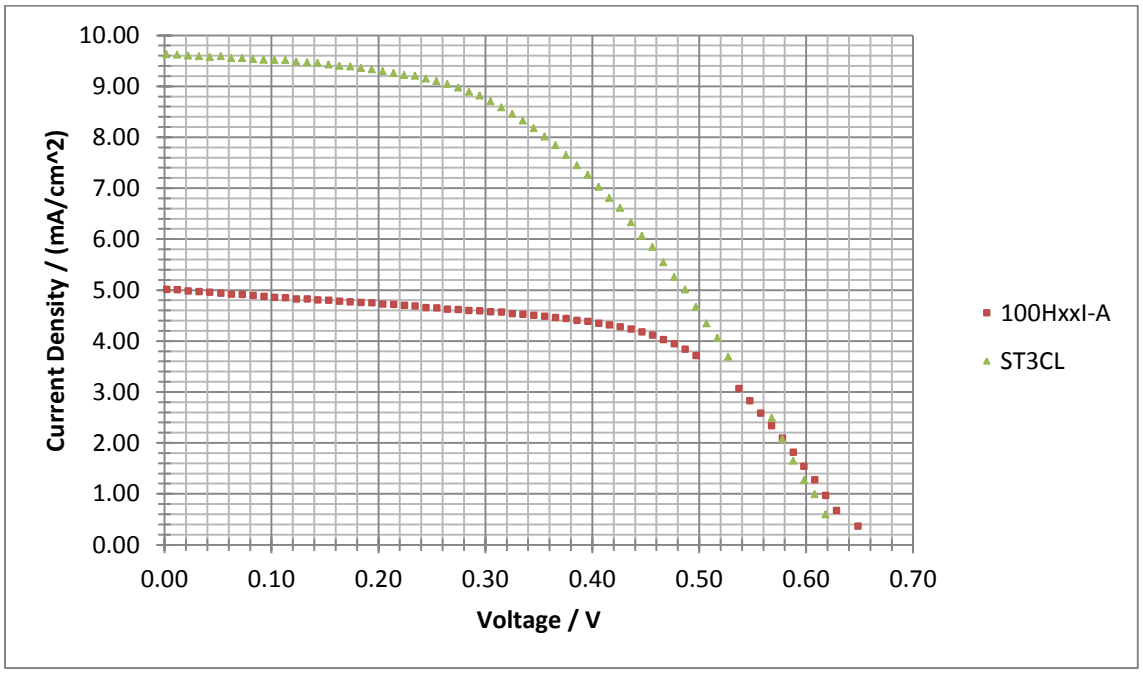

Figure 28. Highest Performing Standard (Acetonitrile Electrolyte) and Polymer Membrane (<100,000 g/mol poly(DADMAI)) Cells

It is apparent some cells have successfully maintained, and even improved upon, their initial power conversion efficiency measurements. Of the poly(DADMAC) trials, 12 cells dropped to less than 15% of their initial PCE. However, 11 cells exceeded their initial PCE measurement. This must be due to insufficient electrolyte penetration at the time of data collection. The cells which show substantial losses in PCE may have been poorly sealed, which may have allowed electrolyte to seep through the Parafilm spacer. Of the 9 remaining cells maintaining at least 15% of their initial PCE and which did not show an increase in PCE, an average PCE retainment of 58.2% was calculated. The variation in results, from 15.4% to 97.2% (when excluding <15% and >100% cells),may be explained by poor cell sealing, but maintenance of 58.2% PCE after 45 days is much better than the few hours shown by acetonitrile electrolytes.

The poly(DADMAI) longevity study is shown in Table 12. No cells in this study show an increase in PCE from initial testing, and only five cells have dropped to below 15% of their initial PCE. Of the remaining 11 cells, an average PCE retainment of 41.0% was calculated. Although this percentage is actually less than that of the poly(DADMAC) longevity study, the measurements show much less variance. If the five cells showing less than 15% retainment are excluded, the % PCE Retained values range from 22.0% to 88.1%. This is a smaller spread than that of poly(DADMAC), which may indicate a higher degree of stability in poly(DADMAI) cells.

Discussion of Effects, Interactions, and Engineering Philosophy

In the variable range tested, only the polymer type and polymer molecular weight were determined to have any statistical significance in the power conversion efficiency. Testing revealed low molecular weight polymers to perform marginally better in poly(DADMAC) trials and quite well in poly(DADMAI) trials. It has been reported that the conductivity of poly(DADMAC) is dependent upon its annealing history, and in particular the drying process [86].

The drying process can modify the structure of the polyelectrolyte complex, which can significantly affect the mobility of charge carriers [86]. This ordered microstructure is thought to

Table 11. Results of poly(DADMAC) Longevity Study

Cell ID	PCE	PCE @ 45 days	% PCE Retained
100H72C-A	0.62	0.05	8.1
100H65C-B	0.90	0.64	71.1
100H74C-C	0.57	0.37	64.9
100H67C-D	1.06	0.09	8.5
100H44C-A	0.89	0.61	68.5
100H59C-B	0.64	1.18	184.4
100H53C-C	0.57	0.01	1.8
100H53C-D	0.65	0.10	15.4
100B66C-A	1.10	1.53	139.1
100B68C-B	0.46	0.50	108.7
100B73C-C	1.00	0.02	2.0
100B71C-D	1.00	0.10	10.0
100B55C-A	0.98	1.32	134.7
100B55C-B	0.72	0.70	97.2
100B69C-C	0.31	0.01	3.2
100B55C-D	0.58	0.78	134.5
450H86C-A	0.65	1.05	161.5
450H73C-B	0.69	0.57	82.6
450H73C-C	0.24	0.02	8.3
450H65C-D	0.79	0.08	10.1
450H59C-A	0.99	0.68	68.7
450H62C-B	0.82	1.10	134.1
450H52C-C	0.36	0.02	5.6
450H52C-D	0.62	0.05	8.1
450B76C-A	0.33	0.71	215.2
450B73C-B	0.18	1.36	755.6
450B74C-C	0.38	0.04	10.5
450B72C-D	0.86	0.21	24.4
450B47C-A	0.22	0.37	168.2
450B55C-B	0.42	0.65	154.8
450B52C-C	0.59	0.02	3.4
450B52C-D	0.58	0.18	31.0

Table 12. Results of poly(DADMAI) Longevity Study

Cell ID	PCE	PCE @ 45 days	% PCE Retained
100H70I-A	1.88	0.04	2.1
100H77I-B	1.38	0.38	27.5
100H66I-C	1.82	0.41	22.5
100H63I-D	1.33	0.61	45.9
100B71I-A	1.09	0.24	22.0
100B77I-B	1.60	1.41	88.1
100B86I-C	1.26	0.70	55.6
100B79I-D	0.67	0.42	62.7
450H70I-A	0.78	0.02	2.6
450H73I-B	0.75	0.05	6.7
450H62I-C	1.01	0.28	27.7
450H70I-D	0.16	0.04	25.0
450B67I-A	1.18	0.16	13.6
450B68I-B	0.75	0.33	44.0
450B64I-C	0.29	0.03	10.3
450C70I-D	1.29	0.38	29.5

arise from the electrostatic interactions present during dehydration [85]. When the polymer is dissolved in water, the chloride ions have dissociated, leaving a multi-charged cationic polymer backbone which assumes the lowest energy configuration possible. This configuration is an elongated chain which may be assumed to form some regular spatial lattice [85]. As the solution is dehydrated, the chloride ions associate with the cationic polymer. Since the dehydration is a slow process, these multi-charged backbones retain their configuration as much as possible during the process. At some point, the polyelectrolyte comes out of solution and retains the micro-structured conformation. This concept seems to be observed in the poly(DADMAC) images of Figures 16 and 17. As noted in the images, the low molecular weight polymer has a much higher degree of ordering compared to the high molecular weight polymer. In the case of iodide diffusion, this characteristic may facilitate ion mobility better than the disorganized entanglement of high molecular weight poly(DADMAC), through both concentration gradient driven diffusion and the Grotthus-type bond exchange mechanism. It is also suggested that high

temperatures can destroy micro-structure ordering [85, 86]. This may confirm the previously unexplained DSC peak on the first temperature scans of poly(DADMAI). If these microstructures exist in the poly(DADMAC) samples, the conformation should be retained in the synthesis of poly(DADMAI) since no heating or cooling was performed until the samples were subjected to DSC temperature scans. The microstructure ordering will also be destroyed if the polymer is dissolved in solvent. In this experiment, the poly(DADMAC) films were submerged in a high molarity iodide solution and it was assumed that since no obvious polymer mass went into solution, the rate of ion exchange exceeded the rate of dissolution. However, it is possible the amount of microstructure ordering was reduced by poly(DADMAC) partial dissolution. It may be prudent for future studies to examine the degree of this microstructural ordering, how it can be controlled, and any impacts it may have on polymer conductivity.

Additionally, poly(DADMAI) was observed to perform better than poly(DADMAC) polymer films (in both molecular weights poly(DADMAI) outperformed poly(DADMAC), with the best results again coming in the low molecular weight variety). The exact reason is difficult to determine, but it is possible the excess iodide gave an increased ability of iodide ions to diffuse across the membrane surface, either through a concentration gradient mechanism or a Grotthus-type mechanism. It is possible both mechanisms worked together to facilitate iodide transport across the membrane surface. The Grotthus mechanism acts as a bond transfer, not a physical ion transfer, and may explain the ability of “ion transfer” to occur so readily through a solid state electrolyte. Instead of physical movement from one side of the membrane to the other, rapid simultaneous bond dissociation and association results in the apparent movement of charge. High void space would allow higher degrees of ionic liquid penetration, which could help both concentration and Grotthus transport. A combined mechanistic transport of actual ions throughout the ionic liquid and a charge-hopping mechanism throughout the

polyelectrolyte microstructure may be the best explanation for this data. Regardless, a noticeable increase in power conversion efficiency was observed, and confirmed.

The alkyl chain length of the imidazolium ionic liquid species was found to be of no statistical significance in this experiment. However, the interaction of ionic liquid with polymer molecular weight was notable, even if not statistically significant. This interaction may be due to the ability of the imidazolium cation to diffuse across the polymer membrane. Steric and ionic actions are surely the cause of this interaction. However, the low molecular weight poly(DADMAC) membranes were found to work best in conjunction with butyl chain length imidazolium iodide, while the low molecular weight poly(DADMAI) worked better with hexyl imidazolium iodide. Therefore, if void space size limited the ability of ionic liquids to diffuse into the electrolyte, it is questionable why hexyl imidazolium iodide performed better than the shorter alkyl chain version. Since longer alkyl chains are known to increase viscosity, the only certain fact is that hexyl imidazolium iodide is more viscous than butyl imidazolium iodide. This should lead to a slight decrease in current and increase in stability for hexyl chains relative to butyl, but instead no statistically relevant data was collected that confirmed this. Since technically the interaction was not significant, it is possible random fluctuations in the data appeared to make a trend look apparent, when in fact there was none.

As previously mentioned, ionic liquid to polymer weight ratio was the only factor deemed insignificant enough to be excluded in secondary trials. Varying from 55% to 75% ionic liquid proved to be an insufficient range to make any difference in performance, so trials were continued at 75% ionic liquid simply to ensure complete filling of the solar cell void space. As it turns out, in final trials it was noted that less ionic liquid may be of more benefit, as excess electrolyte was noted to be escaping the Parafilm® seal and potentially decreasing fill factor and overall cell performance. If the volume of the electrolyte spacer is exceeded, the electrolyte may

leak out and short circuit the cell by contacting the outer conductive coating. It also leads to poor shunt resistance, which is directly related to lower current densities and power conversion efficiencies. This may have occurred.

In the planning stages of this experiment, it was decided to approach the concepts of this research with core engineering philosophy in mind. One of these philosophical goals was to make dye-sensitized solar cell electrolytes out of readily available materials and in methods to facilitate cheap manufacturing procedures in order to lower overall cost. These electrolytes would need to be just stable enough, and provide just enough power output, that when combined with this low cost factor they would be economically feasible in production facilities. This objective was facilitated in every method possible. The polyelectrolyte was developed from readily available polymer and iodide salt compounds, and water was used as a common solvent. The results of the longevity study support the notion that with future work, this process could yield a polyelectrolyte suitable for commercialization.

CHAPTER VII

CONCLUSIONS & FUTURE WORK

Standard Dye-Sensitized Solar Cells

A procedure was developed to produce dye-sensitized solar cells using a commonly referenced iodide/tri-iodide redox reagent in acetonitrile organic solvent. After the procedure was demonstrated to be effective and consistent, ten cells were made as a baseline for comparison to future projects. These cells had average values of 7.8 mA/cm^2 short circuit current density, 0.65 V open circuit voltage, 47% fill factor, and 2.34% power conversion efficiency. Additionally, dye-sensitized solar cells were produced using pure ionic liquid solvent instead of acetonitrile. These ionic liquid electrolyte cells produced output parameters of 9.3 mA/cm^2 short circuit current density, 0.45 open circuit voltage, 30% fill factor, and 1.25% power conversion efficiency.

Poly-electrolyte Membrane Dye-Sensitized Solar Cells

Dye-sensitized solar cells were produced according to the previously developed procedure. The electrolyte in acetonitrile solvent was replaced with an ionic liquid electrolyte in conjunction with a poly(diallyldimethylammonium chloride) polymer membrane. The polymer molecular weight, ionic liquid alkyl chain length, and polymer to ionic liquid weight ratio were varied as high and low parameters in a full factorial experimental design, done with four replicates. The ionic

liquid to polymer weight ratio was deemed statistically insignificant, as well as any interactions with other variables, and it was removed from the second phase of the experiment.

A second polymer, poly(diallyldimethylammonium iodide), was derived from poly(diallyldimethylammonium chloride) and used in the same described procedure. The molecular weight and ionic liquid type were varied in this full factorial experimental design, with four replicates being performed. These results were then combined with the previous data to form a three variable, full factorial experiment. This design was analyzed and both the polymer molecular weight and polymer type were determined to be significant, with poly(DADMAI) of molecular weight <100,000 g/mol showing the highest average solar cell power conversion efficiency at 1.60%. The highest performing cell demonstrated an open circuit voltage of 0.66 V, a short circuit current density of 5.01 mA/cm^2, and a fill factor of 57%, resulting in an overall solar to electric power conversion efficiency of 1.88%.

After 45 days, all poly-electrolyte dye-sensitized solar cells were retested to assess electrolyte stability and cell longevity. Several cells exhibited a drop in PCE to below 15% of the initial PCE, and several poly(DADMAC) cells showed an improvement in PCE. Of the remaining cells, poly(DADMAI) electrolyte membranes retained 41.0% PCE and poly(DADMAC) retained 58.2%. Both of these retainment percentages are much better than the few hours sustained by acetonitrile organic liquid solvent electrolytes.

In conclusion, the polymer poly(DADMAI), in conjunction with 1-hexyl-3-methyl imidazolium iodide ionic liquid solvent (which contains iodide – tri-iodide redox reagent), has proven to be an acceptable electrolyte in dye-sensitized solar cells in terms of both cell stability and overall cell performance.

Future Work

The majority of this project was spent learning the fundamental concepts of dye-sensitized solar cell functioning and developing a process for consistent and functional cell fabrication. Once the procedure was developed, the original experimental design was executed. Now that a working procedure is readily available for future work, there are several future projects that would be beneficial in understanding cell material usage and fabrication effects.

First, the carbon nanotube layer should be optimized for this particular solar cell design. The immediate factors to examine in carbon nanotube electrode production are the thickness of the carbon nanotube deposition layer, the type of carbon nanotube (single, double, or multiwall), and the size of carbon nanotubes (both in length and diameter variations). Advanced carbon nanotube studies may examine the additional of bonded functional groups to carbon nanotubes and other treatment steps to decrease electrical resistance. A comparison of these optimized carbon nanotube counter electrodes could then be compared to similarly designed dye-sensitized solar cells using a platinum counter electrode (as is done at South Dakota State University).

Second, there was discussion regarding the terminology of the “sintering” process of titanium dioxide films. In all the reported literature, the term “sintering” is used to describe the thermal treatment step of the TiO_2 deposition process (referred to in this paper as a thermal treatment, or simply “heating”). This report did not use the term “sinter” since it is an inaccurate description of the process. Particles which are sintered are heated until they bind together, either from melting or a chemical reaction. Titanium dioxide is a catalyst that is stable up to temperatures of 750 °C, so no sintering occurs at 450 °C. What does occur at 450 °C is a re-activation of the catalyst surface to allow dye adherence during dye soaking. If another method of catalyst regeneration were developed, the high temperature heat treatment could be

eliminated and ITO films and flexible polymer substrates could be more readily used in dye-sensitized solar cells. A hypothesized UV treatment could be used to reactivate titanium dioxide films that are deposited using ethanol as a solvent instead of water due to the ability of high energy UV light to degrade ethanol into water and carbon dioxide. Preliminary results using low temperature, room temperature, and UV treated DSSC can be found in Appendix D. It is apparent from the data that UV treatments and low temperature heating is necessary to achieve better cell performance, but continued study on this topic is necessary before any further interpretations can be made.

Now that ionic liquid capabilities have been realized, blends of acetonitrile and ionic liquids are commonly being reported. New work should use this new insight. A blend would allow electrolyte solution to be channel-injected instead of "sandwiched" between the electrodes, which may lead to better fill factors and less current leakage, thereby increasing cell performance. Heating ionic liquid electrolyte may also decrease the viscosity enough to allow for channel-injection. These new electrolytes could be used in conjunction with the results of the poly(DADMAC) – poly(DADMAI) study for composite polyelectrolyte – ionic liquid – acetonitrile electrolytes.

Dr. Sean Hightower of the University of North Dakota chemistry department has been synthesizing a new dye compound using rhenium metal instead of ruthenium metal. A standard cell fabricated with this new dye compound would be the first of its kind. At this time, cells have just been produced using this new dye compound and preliminary data can be found in Appendix E. There may be future work involved with Dr. Hightower using dye-sensitized cell design strategies for use in carbon dioxide reduction instead of solar generated electricity.

One of the most frustrating issues of dye-sensitized solar cell fabrication is related to device sealing. Very few glues or other methods of containment have been developed or

reported that successfully retain the acetonitrile solvent for longer than one day. Any research involving device sealing materials would be of significant importance. This project found and utilized a two-part epoxy material produced by 3M, but there is a significant amount of work that could still be done regarding this particular area of dye-sensitized solar cells.

It was also observed that when using pure ionic liquid solvents in dye-sensitized solar cells, there was a period of time during which cell current production would significantly increase once the cell was illuminated with the solar simulator. It is thought this is a temperature effect, where the increase in temperature decreases the viscosity of the ionic liquid and allows better solvent penetration into the titanium dioxide film. The kinetics of electron transfer may also be increased as temperature increases. A look into these temperature effects could be an interesting endeavor if methods to evaluate such kinetics could be presented. However, it is noteworthy that in the final cell trials (the confirmation tests and the preliminary testing of directly deposited polymer), this period of time to reach steady-state did not exist. Cell currents were immediately at their highest performing level. It is possible this time to reach maximum ability is due to the time it takes for the viscous electrolyte to penetrate the titania and polymer materials, and that if sufficient time is allowed the cell performs well on the first voltage sweep.

APPENDICES

APPENDIX A
DEFINITIONS, SYMBOLS, & UNITS

Active area of solar cell — A — (cm^2)

The area of the solar cell available to absorb energy

Current — I — (mA)

Electron flow measured during data collection
Current density is calculated as current divided by the active area of the solar cell

Current density at maximum power output — J_{max} — (mA / cm^2)

On the current – voltage characteristic curve, the point of maximum power identifies this current

Fill Factor — FF — (unitless)

A scalar denoting the difference between a theoretical cell and the actual cell power output

Incident power from light source — P_{in} — (W / m^2)

The light energy input to the solar cell, under AM1.5 specifications is equal to 1000 W/m^2

Open circuit voltage V_{oc} (V)

The voltage of an illuminated cell in which no current is passing through i.e. $J_{sc} = 0$

Power conversion efficiency PCE (%)

The percentage of light energy converted to electrical energy

Short circuit current density J_{sc} (mA / cm^2)

The current of an illuminated cell in which the cell has been short circuited i.e. $V_{oc} = 0$

Voltage at maximum power output V_{max} (V)

On the current – voltage characteristic curve, the point of maximum power identifies this voltage

APPENDIX B
USEFUL EQUATIONS

Power = current density * voltage

$P_i = J_i V_i$

Current density = current / cell active area

$J_i = I_i / A$

Fill factor = power maximum / (short circuit current density * open circuit voltage)

$FF = P_{max} / (J_{sc} V_{oc})$

Power conversion efficiency = maximum power output / power input *100

$PCE = P_{max} / P_{input} *100$ $P_{input} = 1000\ W/m^2$

$PCE = J_{sc} V_{oc} FF / P_{input} *100$

Theoretical open circuit voltage [88]

$V_{oc} = (nRT/F)*\ln((I_{SC}/I_0) - 1)$

n is an ideality factor between 1 and 2, R is the ideal gas constant, F is Faraday's constant, and I_0 is the reverse saturation current

APPENDIX C
SEM IMAGES CONTAINING DISTANCE SCALES

These images are included as an appendix due to the fact that once the images were scaled down, the incorporated scale was unreadable. These images are here simply for a reference if the polymer samples are desired to be analyzed relative to a distance. All images were recorded at consistent optical zooms (i.e. 35x, 300x, 1000x), so a general idea of the macromolecular characteristics should be realizable.

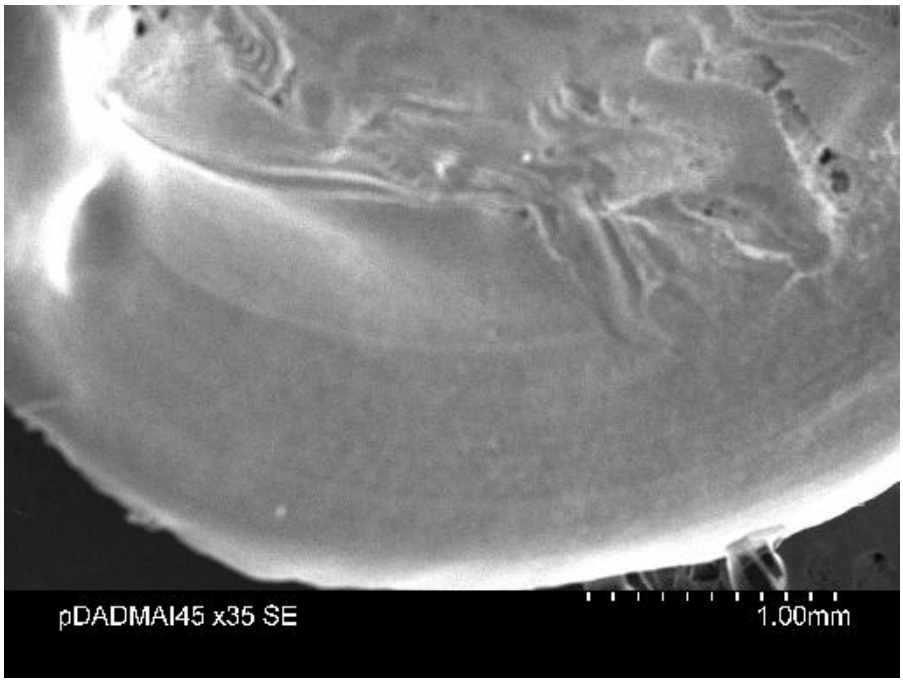

Figure 29. SEM Imaging 35x of poly(DADMAI) MW 400,000 – 500,000 g/mol, Scale Included

Figure 29 shows poly(DADMAI) at 35x zoom. At this magnification, it can be noticed that ridge size in the film surface is on the order of 1 mm in magnitude. These ridge deformations

occur towards the center of the circular membrane, while the outer edges appear to be much smoother. Fine ring formations are noticeable at this magnification, but not distinguishable. In Figure 30, the ring formations take on a thin band appearance which may be an indication of the polymer microscale ordering. Sharp edges of polymer material are identifiable and show where disjoint regions of polymer come together. These regions are approximately 300 µm in diameter.

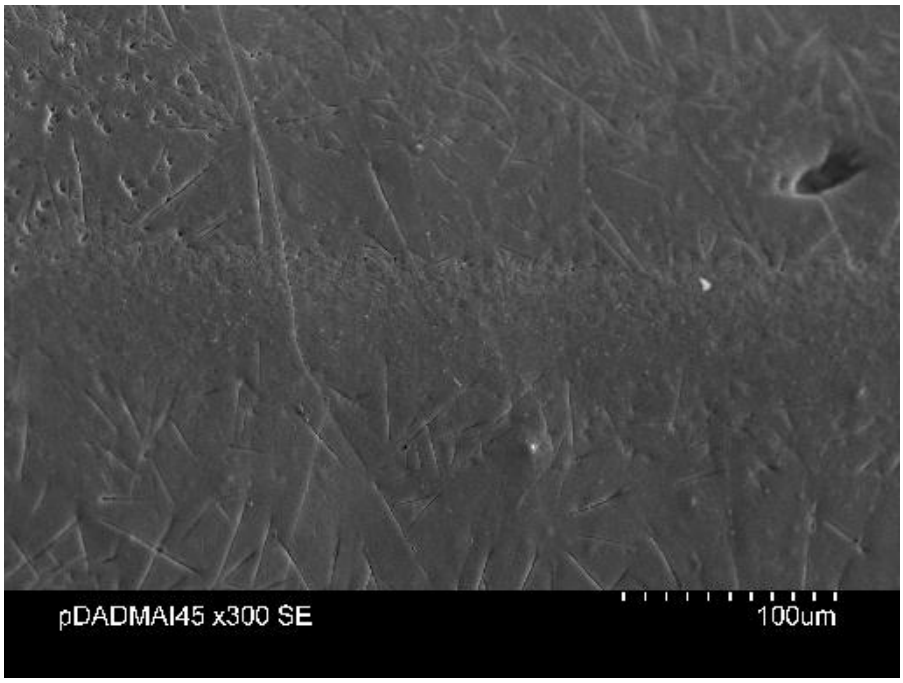

Figure 30. SEM Imaging 300x of poly(DADMAI) MW 400,000 – 500,000 g/mol, Scale Included

In Figure 31, poly(DADMAI) is shown at 1000x magnification. At this level of magnification, the sharp jagged lines separating polymer regions become very distinct. These edge boundaries range in length from 25 µm to hundreds of microns. Band regions may also be viewable, as an apparent boundary exists which segregates a band of larger, smooth microstructure arrays from a band of stubbly looking rough polymer. There appears to be a large number of short, 25 µm edge distinctions between these bands, which may be an indication of the static and electronic forces interacting at this boundary between regions. Further SEM work could delve into the effects these forces play in polymer structuring on the microscale level.

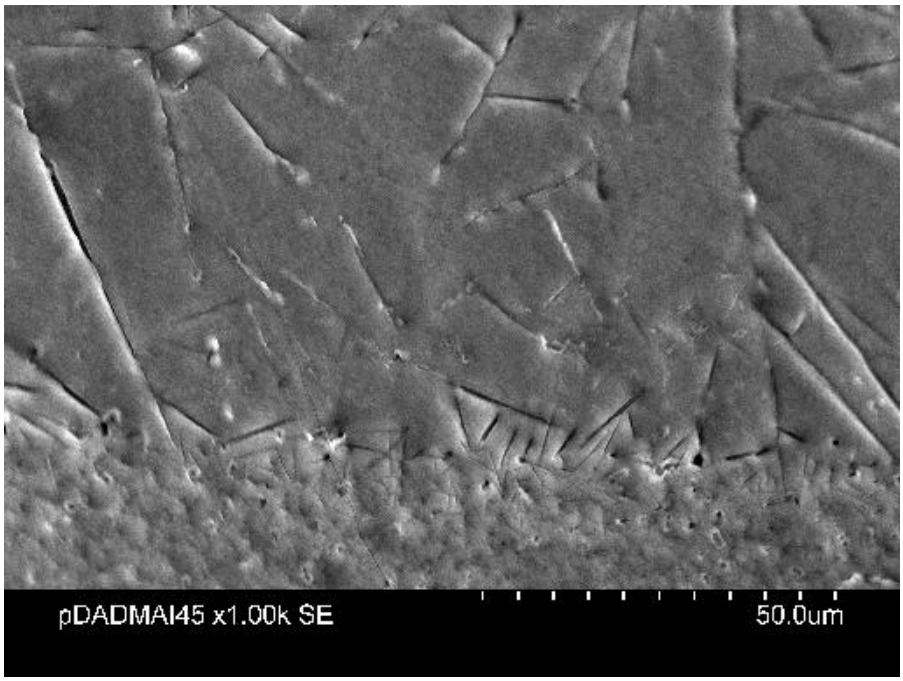

Figure 31. SEM Imaging 1000x of poly(DADMAI) MW 400,000 – 500,000 g/mol, Scale Included

APPENDIX D

PRELIMINARY RESULTS OF UV TREATMENT STUDY

In an attempt to create a process suitable for depositing TiO_2 on flexible plastic substrates, a UV treatment was used to regenerate TiO_2 surface sites instead of the 450 °C high temperature heating cycle. This preliminary study made two replicates of four cell types which were made on ITO coated glass slides.

ITO coated glass slides do not withstand the high temperature heat cycle as well as FTO coated slides. ITO begins to break down at approximately 235 °C. This was determined in the UND laboratory, and is plotted below in Figure 32. It is apparent that heating at the often reported temperature of 450 °C increases resistance substantially and will be detrimental to cell performance.

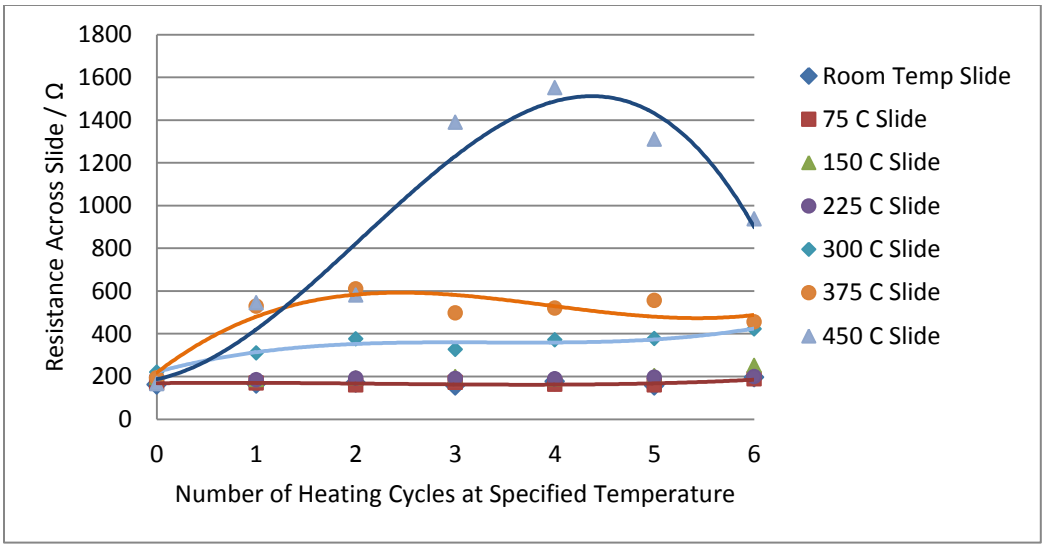

Figure 32. Effect of Temperature and Cyclic Heating on ITO Conductivity

Instead, 210 °C was used as a maximum heat treatment step in DSSC production. Three other cell designs, done in replicate, included a cell which received no treatment (allowed to

dry at room temperature for each TiO_2 deposition), a cell subjected to a UV treatment step to regenerate TiO_2 active sites, and a cell which was subjected to both heat treatment at 210 °C and UV treatment to regenerate TiO_2. UV light intensity was set to 2500 W/m^2 and 15 minutes in duration. A comparison of the current-voltage curves for each cell is shown below in Figure 33. Having only performed two replicates, it is necessary to collect more data before any decisive results are determined. However, it does seem clear that some sort of treatment step is necessary to prevent low fill factors and avoid exceptionally poor cell performance.

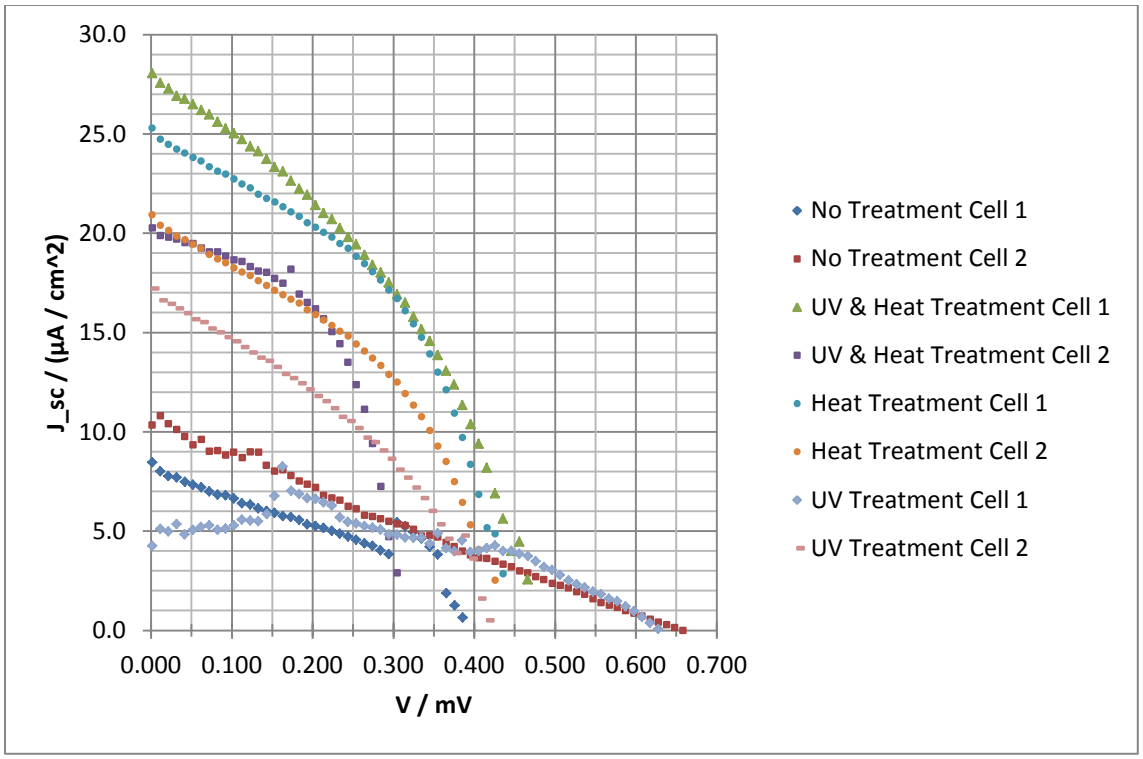

Figure 33. Effect of TiO_2 Post-Treatments on Dye-Sensitized Solar Cell Performance

Note the current density is microamps per square centimeter. This low current density results in extremely low power conversion efficiencies, but different treatment steps do seem to generate a performance effect. Future efforts could look into the response of UV curing duration, intensity, and how polymer films degrade when exposed to high intensity UV light.

APPENDIX E
PRELIMINARY RESULTS OF DSSC USING NOVEL RHENIUM DYE

Dan Black and Dr. Sean Hightower have synthesized a dye compound similar to ruthenium metal based dyes, but instead using the metal rhenium (chemical symbol Re). This dye is expected to have larger voltage capacities and may someday be used in carbon dioxide reduction research.

The exact procedure in this study for the production of standard acetonitrile dye-sensitized solar cells was used to generate new acetonitrile dye-sensitized solar cells using this novel rhenium dye instead of the ruthenium "Black Dye." One set of eight cells was produced and characterized by dark and light current-voltage curves. The illuminated current-voltage curve is shown for one cell in Figure 34 on the next page.

It is apparent the rhenium dye did not function in the dye-sensitized solar cell design. In this instance it is important to graph both the illuminated and dark characterization curves because if only the illuminated graph were to be analyzed, it would appear as if a small current were being produced. In fact, there is no difference between the illuminated and dark curves, so this device fails to generate any electrical current when the dye is illuminated with solar light. This is shown in Figure 34. It is thought this failure is due to either an extremely fast relaxation of the complex (which implies exciton dissociation did not occur) or a lack of physical adherence of the dye to the TiO_2 conducting oxide.

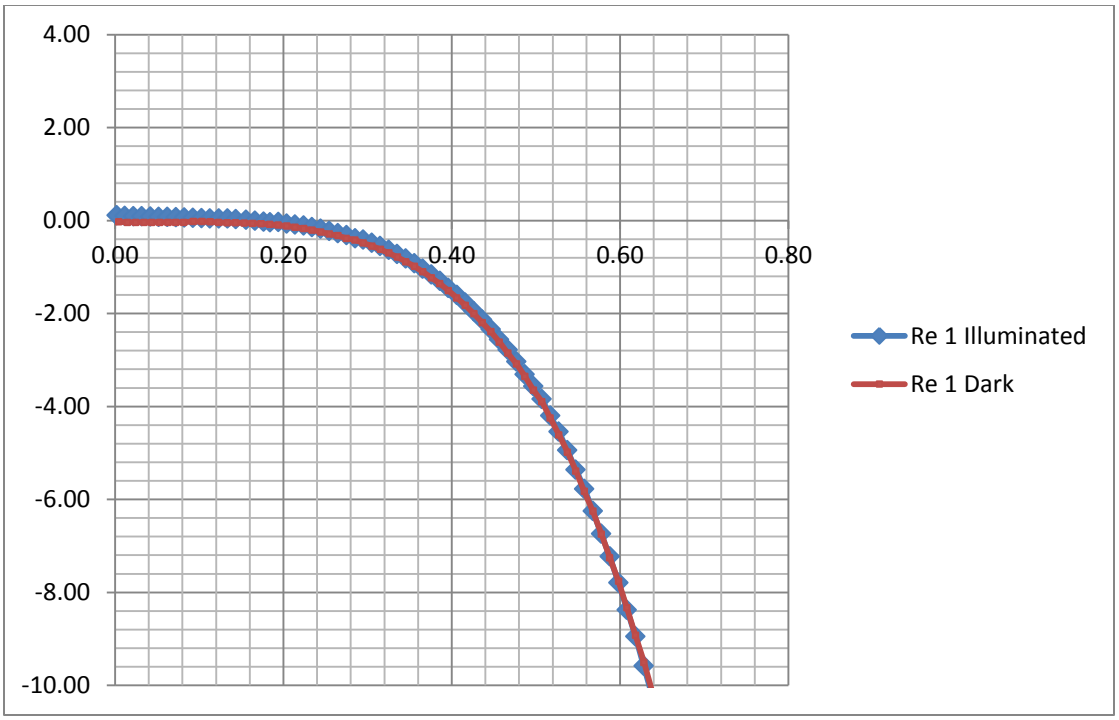

Figure 34. Illuminated and Dark Characterization of Rhenium Dye-Sensitized Solar Cell at 1000 W/m^2 using Acetonitrile Electrolyte Solvent

REFERENCES

1. *Basic Research needs for Solar Energy Utilization.* U.S. Department of Energy. 2005

2. Aimee E. Curtright, M. Granger Morgan, David W. Keith. "Expert Assessments of Future Photovoltaic Technolgies." Environmental Science and Technology 42 (2008): 9031-9038

3. United States Energy Information Administration. Table 5A. Residential Average Monthly Bill by Census Division, and State 2010. 11/03/2011. 01/05/2012 <http://www.eia.gov/electricity/data.cfm#electriccosts>

4. Arnulf Jager-Waldau. "Status of thin film solar cells in research, production, and the market." Solar Energy 77 (2004): 667-678

5. Adolf Goetzberger, Joachim Luther, Gerhard Willeke. "Solar cells: past, present, future." Solar Energy Materials & Solar Cells 74 (2002): 1-11

6. Brian O'Regan, Michael Gratzel. "A low-cost, high-efficiency solar cell based on dye-sensitized colloidal TiO_2 films." Nature 353 (1991): 737-740

7. Martin Green, Keith Emery, Yoshihiro Hishikawa, Wilhem Warta. "Solar Energy Efficiency Tables (version 37)." Progress in Photovoltaics: Research and Applications 19 (2011): 84-92

8. R.D. McConnell. "Assessment of the dye-sensitized solar cell." Renewable and Sustainable Energy Reviews 6 (2002): 273-295

9. Holger Spanggaard, Frederik C. Krebs. "A brief history of the development of organic and polymeric photovoltaics." Solar Energy Materials & Solar Cells 83 (2004): 125-146

10. Aswani Yella, Hsuan-Wei Lee, Hoi Nok Tsao, Chenyi Yi, Aravind Kumar Chandiran, Md.Khaja Nazeeruddin, Eric Wei-Guang Diau, Chen-Yu Yeh, Shaik M. Zakeeruddin, Michael Gratzel. "Porphyrin-Sensitized Solar Cells with Cobalt(II/III)-Based Redox Electrolyte Exceed 12 Percent Efficiency." Science 334 (2011): 629-634

11. Fan-Tai Kong, Song-Yuan Dai, Kong-Jia Wang. "*Review Article* Review of Recent Progress in Dye Sensitized Solar Cells." Advances in OptoElectronics (2007): 75384

12. Md. K. Nazeeruddin, Etienne Baranoff, Michael Gratzel. “Dye-sensitized solar cells: A brief overview.” Solar Energy 85 (2011): 1172-1178

13. Sven Ruhle, Juan Bisquert, David Cahen, Gary Hodes, Arie Zaban. “Electrical and chemical potential distribution in dye-sensitized and similar solar cells in the dark and under illumination.” <http://www.quantsol.unibe.ch/%5Cpub%5Cpub_172.pdf> n.d. accessed 03/20/2012

14. Marko Berginc, Miha Filipic, Ursa Opara Krasovec, Marko Nerat, Andrej Campa, Mateja Hocevar, Franc Smole, Marko Topic. “Electrical Model of Dye-Sensitized Solar Cells.” Proceedings of MIDEM (2009): 251-256

15. S. Wenger, M. Schmid, G. Rothenberger, M. Gratzel, J.O. Schumacher. “Model-Based Optical and Electrical Characterization of Dye-Sensitized Solar Cells.” *Preprint – 24th European Photovoltaic Solar Energy Conference and Exhibition*. Hamburg, Germany (September 2009)

16. Tom Markvart, Luis Castaner. Practical Handbook of Photovoltaics: Fundamentals and Applications. Elsevier Science Ltd., 2003

17. Brian A. Gregg, Mark C. Hanna. “Comparing organic to inorganic photovoltaic cells: Theory, experiment, and simulation.” Journal of Applied Physics. 93 (2003): 3605-3614

18. Anders Hagfeldt, Bengt Didriksson, Tommy Palmqvist, Henrik Lindstrom, Sven Sodergren, Hakan Rensmo, Sten-Eric Lindquist. “Verification of high efficiencies for the Gratzel-cell. A 7% efficient solar cell based on dye-sensitized colloidal TiO_2 films.” Solar Energy Materials & Solar Cells 31 (1994): 481-488

19. Ravi Harikisun, Hans Desilvestro. “Long-term stability of dye solar cells.” Solar Energy 85 (2011):1179-1188

20. A.F. Nogueira, C. Longo, M.A. DePaoli. “Review: Polymers in dye sensitized solar cells: overview and perspectives.” Coordination Chemistry Reviews 248 (2004): 1455-1468

21. S. Balasubaramaniam, K.G. Chittibabu, L. Li, L. Samuelson, J. Kumar, S. Tripathy. Photovoltaic Cells, US Patent US 7323635 B2. January 29, 2008.

22. H. Lindstrom, A. Holmberg, E. Magnusson, L. Malmqvist, A. Hagfeldt. “A new method to make dye-sensitized nanocrystalline solar cells at room temperature.” J. Photochem. Photobiol. A: Chem. 145 (2001): 107-112

23. G.H. Guai, Q.L. Song, Z.S. Lu, Chang-Ming Li. “Effects of multiple heat treatment cycles on structure, optical and electrical properties of indium-tin-oxide thin films.” Surface & Coatings Technology 205 (2011): 2852-2856

24. Li Zhi-hua, Ke Yu-peng, Ren Dong-yan. “Effects of heat treatment on morphological, optical, and electrica properties of ITO films by sol-gel technique.” Trans. Nonferrous Met. Soc. China 18 (2008): 366-371

25. Woon-Hyuk Baek, Mijung Choi, Tae-Sik Yoon, Hyun Ho Lee, Yong-Sang Kim. “Use of fluorine-doped tin oxide instead of indium tin oxide in highly efficient air-fabricated inverted polymer solar cells.” Applied Physics Letters 96 (2010): 133506

26. Beomjin Yoo, Kyungkon Kim, Seung Hoon Lee, Won Mok Kim, Nam-Gyu Park. “ITO/ATO/TiO_2 triple-layered transparent conducting substrates for dye-sensitized solar cells.” Solar Energy Materials & Solar Cells 92 (2008): 873-877

27. Feng Xu, Litao Sun. “Solution-derived ZnO nanostructures for photoanodes of dye-sensitized solar cells.” Energy & Environmental Science. 4 (2011): 818-841

28. Sara E. Coops, Brain C. O’Regan, Piers R. F. Barnes, James R. Durrant. “Parameters Influencing the Efficiency of Electron Injection in Dye-Sensitized Solar Cells.” J. Am. Chem. Soc. 131 (2009): 4808-4818

29. Seigo Ito, Takurou N. Murakami, Pascal Comte, Paul Liska, Carole Gratzel, Mohammad K. Nazeeruddin, Michael Gratzel. “Fabrication of thin film dye sensitized solar cells with solar to electric power conversion efficiencies over 10%.” Thin Solid Films 516 (2008): 4613-4619

30. Curtiss Kovash, Jr. “Handbook for DSSC Fabrication.” South Dakota State University, 2009-2011

31. Kenshiro Uzaki, Terumi Nishimura, Jun Usagawa, Shuzi Hayase. “Dye-Sensitized Solar Cells Consisting of 3D-Electrodes – A Review: Aiming at high Efficiency From the View Point of Light Harvesting and Charge Collection.” Journal of Solar Energy Engineering 132 (2010): 021204

32. Frederik C. Krebs. “Review: Fabrication and processing of polymer solar cells: A review of printing and coating techniques.” Solar Energy Materials & Solar Cells 93 (2009): 394-412

33. Sean E. Shaheen, Rachel Radspinner, Nasser Peyghambarian, Ghassan E. Jabbour. "Fabrication of bulk heterojunction plastic solar cells by screen printing."Applied Physics Letters 79 (2001): 2996 - 2998

34. Hong Lin, Wen-li Wang, Yi-zhu, Xin Li, Jian-bao Li. "New trends for solar cell development and recent progress of dye sensitized solar cells." Front. Mater. Sci. China 3(4) (2009): 345-352

35. Huizhi Zhou, Liqiong Wu, Yurong Gao, Tingli Ma. "Dye-sensitized solar cells using 20 natural dyes as sensitizers." Journal of Photochemistry and Photobiology A: Chemistry (2011), doi:10.1016/j.jphotochem.2011.02.008

36. Mahesh Kumar Bhimwal, K.M. Gangotri. "A comparative study on the performance of photogalvanic cells with different photosensitizers for solar energy conversion and storage: D-Xylose-NaLS systems." Energy 36 (2011): 1324-1331

37. Wangdong Zeng, Yiming Cao, Yu Bai, Yinghui Wang, Yushuai Shi, Min Zhang, Fangfang Wang, Chunyue Pan, Peng Wang. "Efficient Dye-Sensitized Solar Cells with an Organic Photosensitizer Featuring Orderly Conjugated Ethylenedioxythiophene and Dithienosilole Blocks." Chem. Mater. 22 (2010): 1915-1925

38. Jihuai Wu, Zhang Lan, Jianming Lin, Miaoliang Huang, Sancun Hao, Tsugio Sato, Shu Yin. "A Novel Thermosetting Gel Electrolyte for Stable Quasi-Solid-State Dye-Sensitized Solar Cells." Advanced Materials 19 (2007): 4006-4011

39. Michal Sokolsky, Martin Kusko, Michal Kaiser, Julius Cirak. "Fabrication and Characterization of Dye-Sensitized Solar Cells Based on Natural Organic Dyes." Elektroenergetika 4 (2011): 26-29

40. Daibin Kuang, Pascal Comte, Shaik M. Zakeeruddin, Daniel P. Hagberg, Karl martin Karlsson, Licheng Sun, Md.K. Nazeeruddin, Michael Gratzel. "Stable dye-sensitized solar cells based on organic chromophores and ionic liquid electrolyte." Solar Energy 85 (2011): 1189-1194

41. Zhipan Zhang, Seigo Ito, Jacques-E. Moser, Shaik M. Zakeeruddin, and Michael Gratzel. "Influence of Iodide Concentration on the Efficiency and Stability of Dye-Sensitized Solar Cell Containing Non-Volatile Electrolyte." ChemPhysChem 10 (2009): 1834-1838

42. Feng Hao, Hong Lin, Jing Zhang, Dongtian Zhuang, Yizhu Liu, Jianbao Li. "Influence of iodine concentration on the photoelectrochemical performance of dye-sensitized solar cells containing non-volatile electrolyte." Electrochimica Acta 55 (2010): 7225-7229

43. Yao Liu, Anders Hagfeldt, Xu-Rui Xiao, Sten-Eric Lindquist. “Investigation of influence of redox species on the interfacial energetic of a dye-sensitized nanoporous TiO_2 solar cell.” Solar Energy Materials and Solar Cells 55 (1998): 267 – 281

44. Gerrit Boschloo, Leif Haggman, Anders Hagfeldt. “Quantification of the Effect of 4-*tert*-Butylpyridine Addition to I^-/I_3^- Redox Electrolytes in Dye-Sensitized Nanostructured TiO_2 Solar Cells.” J. Phys. Chem. B 110 (2006): 13144-13150

45. Keith E. Johnson, “What’s an Ionic Liquid?” The Electrochemical Society *Interface*. Spring (2007): 38-41

46. Tetsuya Tsuda, Charles L. Hussey. “Electrochemical Applications of Room-Temperature Ionic Liquids.” The Electrochemical Society *Interface*. Spring (2007): 42-49

47. Peng Wang, Shaik M. Zakeeruddin, Ivan Exnar, Michael Gratzel. “High efficiency dye-sensitized nanocrystalline solar cells based on ionic liquid polymer gel electrolyte.” Chem. Commun. (2002): 2972-2973

48. T.M. Wijendra Jayalath Bandara, Piyasiri Ekanayake, M.A.K. Lakshman Dissanayake, Ingvar Albinsson, Bengt-Erik Mellander. “A polymer electrolyte containing ionic liquid for possible applications in photoelectrochemical solar cells.” Journal of Solid State Electrochem 14 (2010): 1221-1226

49. Yu Bai, Yiming Cao, Jing Zhang, Mingkui Wang, Renzhi Li, Peng Wang, Shaik M. Zakeeruddin, Michael Gratzel. “High-performance dye-sensitized solar cells based on solvent-free electrolytes produced from eutectic melts.” Nature Materials 7 (2008): 626-630

50. Po-Yen Chen, Chuan-Pei Lee, R. Vittal, Kuo-Chuan Ho. “A quasi solid-state dye-sensitized solar cell containing binary ionic liquid and polyaniline-loaded carbon black.” Journal of Power Sources 195 (2010): 3933-3938

51. Henriette Santa-Nokki, Sara Busi, Jani Kallioninen, Manu Lahtinen, Jouko Korppi-Tommola. “Quaternary ammonium polyiodides as ionic liquid/soft solid electrolytes in dye-sensitized solar cells.” Journal of Photochemistry and Photobiology A: Chemistry 186 (2007): 29-33

52. Daniel M. Blake, Luc Moens, Daniel Rudnicki, Heidi Pilath. “Lifetime of Imidazolium Salts at Elevated Temperatures.” Journal of Solar Energy Engineering. 128 (2006): 54-57

53. Christopher P. Fredlake, Jacob M. Crosthwaite, Daniel G. Hert, Sudhir N.V.K. Aki, and Joan F. Brennecke. “Thermophysical Properties of Imidazolium-Based Ionic Liquids.” J. Chem. Eng. Data. 49 (2004): 954-964

54. Jilian Nei de Freitas, Ana Flavia Nogueira, Marco-Aurelio De Paoli. “New insights into dye-sensitized solar cells with polymer electrolytes.” Journal of Materials Chemistry 19 (2009): 5279-5294

55. Yanmin Wang. “*Review* Recent research progress on polymer electrolytes for dye-sensitized solar cells.” Solar Energy Materials & Solar Cells 93 (2009): 1167-1175

56. G. Nazmutdinova, S. Sensfuss, M. Schrodner, A. Hinsch, R. Sastrawan, D. Gerhard, S. Himmler, P. Wasserscheid. “Quasi-solid state polymer electrolytes for dye-sensitized solar cells: Effect of the electrolyte components variation on the triiodide ion diffusion properties and charge-transfer resistance at platinum electrode.” Solid State Ionics 177 (2006) 3141-3146

57. Ying Yang, Cong-Hua Zhou, Sheng Xu, Jing Zhang, Su-Juan Wu, hao Hu, Bo-Lei Chen, Qi-Dong Tai, Zheng-Hua Sun, Wei Liu, Xing-Zhong Zhao. “Optimization of a quasi-solid-state dye-sensitized solar cell employing a nanocrystal-polymer composite electrolyte modified with water and ethanol.” Nanotechnology 20 (2009): 105204

58. Zhang Lan, Jihuai Wu, Jianming Lin, Miaoliang Huang. “Application of Thermosetting Organic Solvent Free Polymer Gel Electrolyte in Quasi-Solid-State Dye-Sensitized Solar Cell.” Journal of Applied Polymer Science 116 (2010): 1329-1333

59. Pramod K. Singh, B. Bhattacharya, R.K. Nagarale, S.P. Pandey, Kang-Wook Kim, Hee-Woo Rhee. “Ionic liquid doped poly(N-methyl 4-vinylpyridine iodide) solid polymer electrolyte for dye-sensitized solar cell.” Synthetic Metals 160 (2010): 950-954

60. Jianmei Lu, Feng Yan, John Texter. “Advanced applications of ionic liquids in polymer science.” Progress in Polymer Science. 34 (2009): 431-448

61. Mikhail Gorlov, Lars Kloo. “Ionic liquid electrolytes for dye-sensitized solar cells.” Dalton Transactions. (2008): 2655-2666

62. Anneke Hauch, Andreas Georg. “Diffusion in the electrolyte and charge-transfer reaction at the platinum electrode in dye-sensitized solar cells.” Electrochimica Acta 46 (2001): 3457-3466

63. M. Durr, G. Kron, U. Rau, J.H. Werner, A. Yasuda, G. Nelles. “Diffusion-limited transport of I_3^- through nanoporous TiO_2-polymer gel networks.” Journal of Chemical Physics 121 (2004): 11374-11378

64. Dong-Won Kim, Yeon-Bok Jeong, Sang-Hern Kim, Dong-Yoon Lee, Jae-Sung Song. “Photovoltaic performance of dye-sensitized solar cell assembled with gel polymer electrolyte.” Journal of Power Sources 149 (2005): 112-116

65. Sung Uk Lee, Won Seok Choi, Byungyou Hong. “A comparative study of dye-sensitized solar cells added carbon nanotubes to electrolyte and counter electrodes.” Solar Energy Materials & Solar Cells 94 (2010): 680-685

66. B.K. Koo, D.Y. Lee, H.J. Kim, W.J Lee, J.S. Song, H.J. Kim. “Seasoning effect of dye-sensitized solar cells with different counter electrodes.” J. Electroceram. 17 (2006): 79-82

67. Marcelo V. Migliorini, Ricardo K. Donato, Moises A. Benegnu, Jairton Dupont, Reinaldo S. Goncalves, Henri S. Schrekker. “Imidazolium ionic liquid-water mixtures: The formation of a new species that inhibits the electrocatalytical charge transfer processes on a platinum surface.” Catalysis Communications 9 (2008): 971-975

68. T. Denaro, V. Baglio, M. Girolamo, V. Antonucci, A.S. Arico, F. Matteucci. R. Ornelas. “Investigation of low cost carbonaceous materials for applications as counter electrodes in dye-sensitized solar cells.”J. Appl. Electrochem. 39 (2009): 2173-2179

69. Zhongrui Li, Hom R. Kandel, Enkeleda Dervishi, Viney Saini, Alexandru S. Biris, Dan Lupu. “Does the wall number of carbon nanotubes matter as conductive transparent material?” Applied Physics Letters 91 (2007): 053115

70. Won Jae Lee, Easwaramoorthi Ramasamy, Dong Yoon Lee, Jae Sung Song. “Efficienct Dye-Sensitized Solar Cells with Catalytic Multiwall Carbon Nanotube Counter Electrodes.” Applied Materials & Interfaces 1 (2009)1145-1149

71. Zhongrui Li, Hom R. Kandel, Enkeleda Dervishi, Viney Saini, Yang Xu, Alexandru R. Biris, Dan Lupu, Gregory Salamo. “Comparative Study on Different Carbon Nanotube Materials in Terms of Transparent Conductive Coatings.” Langmuir 24 (2008): 2655-2662

72. Matthew Meitl, Yangxin Zhou, Ahshu Gaur, Seokwoo Jeon, Monica Usrey, Michael Strano, John Rogers. “Solution Casting and Transfer Printing Single-Walled Carbon Nanotube Films.” Nano Letters 4 (2004) 1643-1647

73. Jessika E. Trancik, Scott Calabrese Barton, James Hone. “Transparent and Catalytic Carbon Nanotube Films.” Nano Letters 8 (2008) 982-987

74. S. Hwang, J. Moon, S. Lee, D.-H. Kim, D. Lee, W. Choi, and M. Jeon. “Carbon nanotubes as counter electrode for dye-sensitized solar cells.” Electronics Letters 43 (2007) 1455-1456

75. M. Kang, Y. Han, H. Choi, and M. Jeon. “Two-step heat treatment of carbon nanotube based paste as counter electrode of dye-sensitized solar cells.” Electronics Letters 46 (2010) 1509-1510

76. Di Wei, Husnu Emrah Unalan, Dongxue han, Qixian Zhang, Li Niu, Gehan Amaratunga, Tapani Ryhanen. “A solid-state dye-sensitized solar cell based on a novel ionic liquid gel and ZnO nanoparticles on a flexible polymer substrate.” Nanotechnology 19 (2008): 424006

77. Ryuji Kawano, Toru Katakabe, Hironobu Shimosawa, Md. Khaja Nazeeruddin, Michael Gratzel, Hiroshi Matsui, Takayuki Kitamura, Nobuo Tanabe, Masayoshi Watanabe. “Solid-state dye-sensitized solar cells using polymerized ionic liquid electrolyte with platinum-free counter electrode.” Physical Chemistry Chemical Physics 12 (2010): 1916-1921

78. Takeshi Yamaguchi, Yuki Uchida, Shinya Agatsuma, Hironori Arakawa. “Series-connected tandem dye-sensitized solar cell for improving efficiency to more than 10%.” Solar Energy Materials & Solar Cells. 93 (2009): 733-736

79. M. Durr, A. Bamedi, A. Yasuda, G. Nelles. “Tandem dye-sensitized solar cell for improved power conversion efficiencies.” Applied Physics Letters 84 (2004): 3397-3399

80. Solar Light Company, Inc. “LS1000 Solar Simulator and 1 Kw Power Supply Users Manual.” Solar Light Company, Inc., Glenside, PA, October 6, 2006

81. Herbert Dautzenberg, Eckhard Gornitz, Werner Jaeger. “Synthesis and characterization of poly(diallyldimethylammonium chloride) in a broad range of molecular weight.” Macromol. Chem. Phys. 199 (1998): 1561-1571

82. Seon Jeong Kim, Seoung Gil Yoon, In Young Kim, Sun I. Kim. “Swelling Characterization of the Semi-interpenetrating Polymer Network Hydrogels Composed of Chitosan and Poly(diallyldimethylammonium chloride).” Journal of Applied Polymer Science 91 (2004): 2876-2880

83. Jun Chen, Mingzhu Liu, Hongliang Liu, Liwei Ma, Chunmei Gao, Siying Zhu, Shaopeng Zhang. “Synthesis and properties of thermo- and pH-sensitive poly(diallyldimethylammounium chloride)/poly(N,N-diethylacrylamide) semi-IPN hydrogel.” Chemical Engineering Journal 159 (2010): 247-256

84. Frank Caruso, Helmuth Mohwald. “Preparation and Characterization of Ordered Nanoparticle and Polymer Composite Multilayers on Colloids.” Langmuir 15 (1999): 8276-8281

85. Eugene L. Sokolov, Fengji Yeh, Alexei Khokhlov, Benjamin Chu. “Nanoscale Supramoleculare Ordering in Gel-Surfactant Complexes: Sodium Alkyl Sulfates in Poly(diallyldimethylammonium Chloride).” Langmuir 12 (1996): 6229-6234

86. Arpad W. Imre, Monika Shonhoff, and Cornelia Cramer. “A conductivity study and calorimetric analysis of dried poly(sodium 4-styrene sulfonate)/poly(diallyldimethylammounium chloride) polyelectrolyte complexes.” The Journal of Chemical Physics 128 (2008): 134905-1 – 134905-8

87. S.C. Yeo, A. Eisenberg. “Effect of Ion Placement and Structure on Properties of Plasticized Polyelectrolytes.” J. Macromol. Sci. – Phys. B13(3) (1977): 441-484

88. Jef Poortmans, Vladimir Arkhipov. Thin Film Solar Cells: Fabrication, Characterization, and Applications. John Wiley & Sons, Ltd., 2006